Risto Ojajärvi

ELECTRON-PHONON INTERACTION IN FLAT-BAND SUPERCONDUCTIVITY

Master's thesis

Supervisor:
Tero Heikkilä

UNIVERSITY OF JYVÄSKYLÄ
DEPARTMENT OF PHYSICS

19th May, 2017

Tiivistelmä

Parhaiten tunnettu suprajohtavuuden syntymekanismi perustuu fononien välittämään vetovoimaan elektronien välillä. Tässä tutkielmassa tutkin fononien välittämää suprajohtavuutta systeemeissä, jossa elektronivyöt ovat tasomaisia. Tasovyöllä elektronien dispersio on erittäin heikko, jolloin tilatiheys on tavanomaista suurempi. Tämän takia suprajohtavuus tasovyöllä on tavanomaista voimakkaampi silloin kun elektronien välinen vetovoima on heikko.

Eliashbergin teoria on elektroni–fononi-suprajohtavuuden teoria, joka ottaa luonnollisella tavalla fononien äärellisen nopeuden huomioon elektronien välisessä vuorovaikutuksessa. Pohjustuksena tasovyösuprajohtavuuteen perehdyn Eliashbergin teoriaan ensin Fermi-pinnalla. Tarkastelen myös Coulombin vuorovaikutuksen sekä fononispektrin vaikutusta Fermi-pinnan suprajohtavuuteen. Ratkon Eliashbergin teorian integraaliyhtälöryhmää eri tapauksissa numeerisesti.

Tutkielmassa sovellan Eliashbergin teoriaa tasovyömallille ja johdan uusia tuloksia tässä mallissa. Redusoimalla Eliashbergin teorian staattisen vuorovaikutuksen rajalle saan selville tasovyön BCS-vuorovaikutusparametrin mikroskooppisten suureiden avulla ilmaistuna. Huomaan kriittisen lämpötilan olevan heikolla kytkennällä kytkinvakion suhteen lineaarinen, mikä vastaa aiempaa BCS-teorian ennustetta. Tämä lineaarisuus säilyy myös äärellisen litteillä dispersioilla. Tarkastelen myös tasovyöllä fononispektrin ja Coulombin vuorovaikutuksen vaikutusta suprajohtavuuteen.

Konkreettisena esimerkkinä tasovyösysteemistä tutkin romboedrisen grafiitin pintatiloja. Romboedrisen grafiitin elektronista rakennetta tarkastelen matalan energian rajalla ja esittelen pintatilojen matemaattisen johdon. Muotoilen Eliashbergin teorian itsekonsistenssiyhtälöt romboedriselle grafiitille matriisimuodossa, mikä on myös uusi tulos.

Avainsanat: suprajohtavuus, elektroni-fononi-vuorovaikutus, Eliashbergin teoria, tasovyö, romboedrinen grafiitti, pintatilat

Abstract

The best-known mechanism for superconductivity is the phonon-mediated attractive interaction between electrons. In this thesis, I study phonon-mediated superconductivity in systems containing flat electronic bands. In the flat band, the electronic dispersion is very weak, which corresponds to a high density of states. For this reason, superconductivity in the flat band is stronger than in the Fermi surface when the attractive interaction is weak.

The Eliashberg theory is a rigorous theoretical framework of electron-phonon superconductivity, which takes naturally into account the finite speed of the phonons in the interaction between the electrons. As a preparation for the study of the flat band superconductivity, I review the Eliashberg theory for the Fermi surface. I also consider the effects of the Coulomb interaction and of different phonon spectra to superconductivity in the Fermi surface. I solve the self-consistency equations of the Eliashberg theory numerically.

I apply the Eliashberg theory to a flat band model, in which I obtain novel results. By reducing the Eliashberg theory to a limit of a static interaction, I find the flat-band BCS interaction constant in terms of microscopic parameters. I also find the critical temperature to be linear with respect to the interaction constant, which agrees with the earlier results based on the BCS theory. I examine the effects of the different phonon spectra and the Coulomb interaction on superconductivity also in the flat band.

As a concrete example of a flat band system I study the surface states of rhombohedral graphite. I present the electronic structure of rhombohedral graphite within the low-energy approximation and contruct the surface states. I obtain some new results by formulating the self-consistency equations of the Eliashberg theory for the rhombohedral graphite in an matrix form.

Keywords: superconductivity, electron-phonon interaction, Eliashberg theory, flat band, rombohedral graphite, surface states

Contents

1 Introduction

In this thesis, I study superconductivity in condensed matter systems with the flat-band electronic dispersion. Specifically, I consider the electron-phonon interaction in these systems.

Superconductivity is a state of matter in which the electronic resistance is exactly zero. Superconductivity was discovered experimentally in 1911, but it took more than forty years before its microscopic origin was understood. A clue to understanding superconductivity was found in 1950, when two separate experiments with isotopes of mercury provided evidence that the temperature above which superconductivity vanishes depends on the choice of the isotope[1, 2]. This was taken to imply that lattice vibrations, or more formally, phonons, are involved in superconductivity[3]. It was then shown by Fröhlich[4] and Pines[5] that an exchange of a virtual phonon may cause an attractive force between two electrons. Finally, in 1957 John Bardeen, Leon Cooper and Robert Schrieffer published a theory which showed that such an attractive interaction makes pairs of electrons form bound states and condense into a superconducting state[6]. This theory is commonly known as the BCS theory, and for it, Bardeen, Cooper and Schrieffer received the 1972 Nobel prize in physics.

In the BCS theory, the precise form of the interaction between electrons and phonons is not utilized. The BCS theory is more focused on the consequences of the attractive interaction than the details of the interaction mechanism itself. After the publication of the BCS theory, the details of the interaction were worked out by a number of people, and the electron-phonon superconductivity theory was laid on a rigourous foundation. In 1958 Migdal developed the perturbation theory to handle the electron-phonon interactions in the normal state[7] and in 1960 Eliashberg[8] and Nambu[9] extended it to the superconducting state. The Coulomb interaction was included by Bogoliubov et al.[10] and Morel and Anderson[11]. This whole theoretical framework of the electron-phonon superconductivity is referred in this thesis as the Eliashberg theory.

Based on the BCS theory, we can examine which properties of the material determine if it is a good superconductor, with a high critical temperature. In particular, we learn that the strength of the superconductivity in metals depends on the electronic density of states at the Fermi level. The density of states is determined by the shape of the electronic dispersion. The flatter the dispersion, the higher the density of states. The extreme case is when the dispersion vanishes completely and a flat-band spectrum is obtained. The BCS theory on flat bands has been recently studied and it indeed was found that the superconductivity is enhanced on them compared to the case with an ordinary Fermi surface[12].

The purpose of this thesis is to study the flat-band superconductivity from the point

of view of the Eliashberg theory; to see if the enhanced superconductivity is present also in this formulation and if it depends on the specific form of the interactions. To my knowledge, this has not been done analytically before, so I obtain some novel results. I begin by reviewing the Eliashberg theory first in the metallic systems with the Fermi surface. After that, I apply the theory to the flat band. I find that the BCS results for the flat band are replicated in the Eliashberg theory when the interactions are weak and that the BCS interaction parameter can be obtained by reducing the theory to the BCS limit. I also take into account the Coulomb interaction and find that it can be included in the flat band by using a pseudopotential in a same way as for the Fermi surface. The Coulomb interaction opposes superconductivity, but I find that its effect is reduced with the increasing size of the flat band.

The flat-band spectrum is obtained on many graphene-based systems. In this thesis, we choose to study surface states of rhombohedral graphite as an example. This is partly motivated by the experimental signs of high-temperature superconductivity found in graphite[13, 14] and partly by the interesting topological properties of the rhombohedral graphite[15]. In this case the Eliashberg theory cannot be reduced into a simple set of equations, but I present a numerical scheme for the solution.

In nature, graphite occurs in a somewhat disorganized state and its electronical properties do not usually match the pure rhombohedral graphite studied in this thesis. One can then ask how relevant the study of the electronic properties arising from such specific arrangement is. The answer is that with the rapidly developing microfabrication techniques, graphite with purely rhombohedral stacking can be artificially made[16] and thus the possible advantages of the flat-band dispersion are becoming realizable.

2 Superconductivity in the BCS theory

As I study Eliashberg theory as a way of going beyond and clarifying the approximations of BCS theory, it is natural to first describe the basic structure of the simpler BCS theory. However, before doing even that, a brief introduction to the physics of electrons and phonons is given.

2.1 Electrons and phonons

In the energy scales typically studied in solid state physics, matter is composed of atomic nuclei and electrons, the number of which are fixed. In this situation, the only interaction of importance is the Coulomb interaction. Schematically, we can then take as our starting point the Hamiltonian which describes the Coulomb interaction between these basic constituents,[17]

$$\hat{H} = \hat{H}_{\mathrm{n}} + \hat{H}_{\mathrm{e}} + \hat{H}_{\mathrm{n\text{-}n}} + \hat{H}_{\mathrm{n\text{-}e}} + \hat{H}_{\mathrm{e\text{-}e}}, \tag{2.1}$$

where $\hat{H}_{\mathrm{n}}$ and $\hat{H}_{\mathrm{e}}$ are the kinetic energy operators of the nuclei and the electrons. $\hat{H}_{\mathrm{e\text{-}e}}$, $\hat{H}_{\mathrm{n\text{-}n}}$ and $\hat{H}_{\mathrm{n\text{-}e}}$ describe the electron–electron, nucleus–nucleus and nucleus–electron Coulomb interactions, respectively.

In this work, the Planck and Boltzmann constants are set to unity,

$$\hbar = k_B = 1, \tag{2.2}$$

so that both frequency and temperature have the unit of energy. In some equations the Boltzmann constant k_B is written to make a connection with the conventional form of the equation.

To separate the Hamiltonian (2.1) into bite-size components, we notice that the proton mass is 1800 times larger than the electron mass and consequently, that the nuclei move much slower than electrons. For this reason we can use the Born-Oppenheimer approximation, according to which the electrons react instantly to the changes in the potential caused by the nuclei. In other words, the potential created by the nuclei changes adiabatically with respect to the electronic system. With the nuclei effectively stationary, the Schrödinger equation can be solved independently for the electrons and the electronic energy of the system can be calculated for the nuclei in different positions. The equilibrium positions of the nuclei can then be found by minimizing the total energy. In this thesis, the equilibrium positions of the nuclei are assumed to form a periodic lattice.

With the nuclei at their equilibrium positions, the electrons see them as a periodic potential, and the electronic band structure can be calculated with help of Bloch's theorem[18]. Assuming only one band with dispersion $\varepsilon_{\mathbf{p}}$, the grand canonical Hamiltonian

for the electrons is

$$H_{\mathrm{e}} = \sum_{\mathbf{p}\sigma} (\varepsilon_{\mathbf{p}} - \mu) c^{\dagger}_{\mathbf{p}\sigma} c_{\mathbf{p}\sigma}, \tag{2.3}$$

where $c_{\mathbf{p}\sigma}$ and $c^{\dagger}_{\mathbf{p}\sigma}$ are the annihilation and creation operators for electrons with momentum $\mathbf{p}$ and spin σ, respectively. As electrons are fermions, they obey the anticommutation relation:

$$\left\{ c_{\mathbf{p}\sigma}, c^{\dagger}_{\mathbf{p}'\sigma'} \right\} = \delta(\mathbf{p}-\mathbf{p}')\delta_{\sigma\sigma'}. \tag{2.4}$$

The chemical potential μ determines the electron number, which is fixed. As the electron dispersion will always appear together with μ, we also define a shifted dispersion

$$\xi_{\mathbf{p}} = \varepsilon_{\mathbf{p}} - \mu. \tag{2.5}$$

Allowing the nuclei to move, the total energy of the nuclei-electron system can calculated with the nuclei slightly shifted from their equilibrium positions. The total energy can then be expanded up to a harmonic approximation with respect to the positions of of the nuclei. The nuclei thus become a set of coupled harmonic oscillators. The corresponding system of equations can be diagonalized as a set of independent harmonic oscillators. These independent oscillators represent the lattice vibrations with well-defined (crystal) momentum and are known as phonons. The Hamiltonian for them is

$$H_{\mathrm{ph}} = \sum_{\mathbf{q}} \omega_{\mathbf{q}} b^{\dagger}_{\mathbf{q}} b_{\mathbf{q}}, \tag{2.6}$$

where $\omega_{\mathbf{q}}$ is the phonon dispersion and the sum is cut off at some maximum frequency q_M. Annihilation and creation operator for a phonon with (crystal) momentum $\mathbf{q}$ are $b_{\mathbf{q}}$ and $b^{\dagger}_{\mathbf{q}}$. There is also an implicit summation over the different branches of the phonon dispersion. Phonons are bosonic and obey the commutation relation,

$$\left[b_{\mathbf{q}}, b^{\dagger}_{\mathbf{q}'} \right] = \delta(\mathbf{q} - \mathbf{q}'). \tag{2.7}$$

The branches of the phonon dispersion can be divided into two categories, optical and acoustic. The energy of the optical phonons doesn't depend much on their momentum and can be represented by the Einstein model, $\omega_q = \omega_E$, in which the energy of the phonon ω_E is completely independent of its momentum. For the acoustic phonons the energy depends linearly on q with small $\mathbf{q}$. In this thesis, acoustic phonons are represented by the Debye model $\omega_{\mathbf{q}} = cq$, with c the speed of sound in the material. The cutoff energy in the Debye model is ω_D.

If the Born-Oppenheimer approximation is relaxed, so that the electrons do not respond instantly to the movements of the ions, we must add a coupling between electrons and phonons described by the term

$$H_{\mathrm{e\text{–}p}} = \sum_{\mathbf{p}\sigma\mathbf{q}} g_{\mathbf{q}} \left(b_{\mathbf{q}} + b^{\dagger}_{-\mathbf{q}} \right) c^{\dagger}_{\mathbf{p}+\mathbf{q}\sigma} c_{\mathbf{p}\sigma}, \tag{2.8}$$

where $g_{\mathbf{q}}$ is electron-phonon coupling constant. This term accounts for the fact that when a phonon is introduced into the system, the periodic potential seen by the electrons changes, and the electrons originally on their eigenstates have a finite propability of scattering to a different state. The energy difference between the incoming and outgoing electrons is released into or absorbed from the phonon system, depending on the sign. Because this coupling only arises as a correction to the adiabatic approximation, it is usually small enough to be treated as a perturbation.

Combining the above terms, we arrive at the Hamiltonian

$$\hat{H} = \hat{H}_{\text{e}} + \hat{H}_{\text{ph}} + \hat{H}_{\text{e-ph}} + \hat{H}_{\text{e-e}}, \tag{2.9}$$

which should be contrasted with the Hamiltonian we began with. The ions are not present in this Hamiltonian anymore, but their properties are reflected in the phononic and electronic dispersion relations. There is also the average Coulomb attraction between the electrons and positively charged nuclei, which is not described by the above Hamiltonian. However, the system is assumed to be electronically neutral, so the attraction between ions and the electrons will balance with the average repulsion between the electrons. Thus this term can be included by modifying the repulsive term $\hat{H}_{\text{e-e}}$. This problem is considered briefly in Sec. 5.4.

2.2 Interactions in BCS theory

Superconductivity is a state of the electronic system, so we are interested in interactions between two electrons, not with one electron and a phonon as in (2.8). We would like to obtain the form of an effective interaction between the electrons, mediated by phonons. It is possible to work within the second quantization formalism to obtain this interaction in the lowest order by doing a Schrieffer-Wolff transformation. In the Schrieff-Wolff transformation, the system is rotated in a such a way that in the first order in coupling g, electrons and phonons become non-interacting with each other[19]. After this transformation, the interaction between an electron and a phonon gets translated as an interaction between two electrons:

$$H_{\text{int}} = \sum_{\mathbf{p}\sigma\mathbf{p}'\sigma'\mathbf{q}} |g_{\mathbf{q}}|^2 \frac{2\omega_{\mathbf{q}}}{(\varepsilon_{\mathbf{k}+\mathbf{q}} - \varepsilon_{\mathbf{p}})^2 - \omega_{\mathbf{q}}^2} c^\dagger_{\mathbf{p}'-\mathbf{q}\sigma'} c^\dagger_{\mathbf{p}+\mathbf{q}\sigma} c_{\mathbf{p}\sigma} c_{\mathbf{p}'\sigma'}. \tag{2.10}$$

The denominator of the potential is negative if

$$|\varepsilon_{\mathbf{p}} - \varepsilon_{\mathbf{p}'}| < \omega_{\mathbf{q}}, \tag{2.11}$$

meaning that the phonons create an attraction between the electrons with similar energies and the attractive region is determined by the Debye frequency ω_D.

The details of the attractive interaction are not used in the BCS theory. Furthermore, we are only interested in the effects near the Fermi surface, and for that purpose we can

approximate the interaction with a double step potential of the form

$$V_{\mathbf{p}\mathbf{p}'} = -V\,\Theta(|\varepsilon_{\mathbf{p}} - \varepsilon_{\mathrm{F}}| - \omega_{\mathrm{D}})\,\Theta(|\varepsilon_{\mathbf{p}'} - \varepsilon_{\mathrm{F}}| - \omega_{\mathrm{D}}), \tag{2.12}$$

where Θ is the Heaviside step function, and the interaction strength is determined by a parameter $V > 0$. This simple form still manages to capture the most important details of the interaction; it is attractive between electrons of similar energies and has a cutoff at Debye energy. It is also confined to act only near the Fermi surface. The repulsive part of the phonon-mediated interaction is omitted, as it doesn't change the qualitative situation.

If we add the Coulomb interaction to Eq. (2.10), the attraction is weakened a bit, but the total interaction still remains attractive when the inequality (2.11) is satisfied. Coulomb interaction is difficult to handle in a satisfactory way within the BCS theory, but it will be considered in more detail with the Eliashberg theory. For now the Coulomb interaction can be considered just to reduce the strength of the effective interaction V, and thus be included in the effective BCS interaction.

2.3 Superconducting mean field

With the simplified interaction model Eq. (2.12), the electronic Hamiltonian can be written as

$$H = \sum_{\mathbf{p},\sigma} \varepsilon_{\mathbf{p}} c^{\dagger}_{\mathbf{p}\sigma} c_{\mathbf{p}\sigma} + \sum_{\mathbf{p},\mathbf{p}',\mathbf{q},\sigma,\sigma'} V_{\mathbf{p}\mathbf{p}'} c^{\dagger}_{\mathbf{p}'-\mathbf{q}\sigma'} c^{\dagger}_{\mathbf{p}+\mathbf{q}\sigma} c_{\mathbf{p}\sigma} c_{\mathbf{p}'\sigma'}. \tag{2.13}$$

The task now would be to obtain the ground state wavefunction and the excitation spectrum. The difficulty is that the interaction is quartic in field operators. Usually the only Hamiltonians that can be diagonalized in system with many particles are the ones with quadratic (one-particle) interactions. Therefore, we need to do a mean field approximation and decompose the quartic term into a sum of quadratic terms.

In the mean field approximation, we also choose which combinations of the operators obtain a non-vanishing expectation value. Therefore, the form of our ansatz determines the for example the ensuing symmetry of the superconducting order parameter. For s-wave (isotropic) superconductivity, the order parameter connects the states with opposite momenta and spin, and the approximate interaction Hamiltonian is

$$H_{\mathrm{int}} = \sum_{\mathbf{p},\mathbf{p}',\sigma} V_{\mathbf{p}\mathbf{p}'} \left\{ \langle c_{\mathbf{p}'\sigma} c_{-\mathbf{p}'\bar{\sigma}} \rangle\, c^{\dagger}_{-\mathbf{p}\bar{\sigma}} c^{\dagger}_{\mathbf{p}\sigma} - \left\langle c_{\mathbf{p}'\sigma} c_{-\mathbf{p}'\bar{\sigma}} \right\rangle^{*} c_{\mathbf{p}\sigma} c_{-\mathbf{p}\bar{\sigma}} \right\}, \tag{2.14}$$

where a constant (non-operator) term has been omitted, as it is usually relevant only in comparing the total energy of the superconducting state to other phases.

The gap function is then defined as

$$\Delta_{\mathbf{k}} = \sum_{\mathbf{k}'} V_{\mathbf{k}\mathbf{k}'} \langle c_{\mathbf{p}'\uparrow} c_{-\mathbf{p}'\downarrow} \rangle\,. \tag{2.15}$$

The pair amplitude Δ is the order parameter in the superconducting state. It is zero above the critical temperature. The interaction part of the Hamiltonian can be written with Δ as

$$H_{\text{int}} = \sum_{\mathbf{p}\sigma} \left\{ \Delta_{\mathbf{p}} c^{\dagger}_{-\mathbf{p}\bar{\sigma}} c^{\dagger}_{\mathbf{p}\sigma} - \Delta^{*}_{\mathbf{p}} c_{\mathbf{p}\sigma} c_{-\mathbf{p}\bar{\sigma}} \right\}, \tag{2.16}$$

where the strength of the mean-field interaction now depends on Δ.

2.4 Solving the mean-field Hamiltonian

To diagonalize the Hamiltonian with the interaction (2.16), it is useful to group operators with opposite spin and momentum in a pseudospinor structure

$$\Psi_{\mathbf{p}} = \begin{pmatrix} c_{\mathbf{p}\uparrow} \\ c^{\dagger}_{-\mathbf{k}\downarrow} \end{pmatrix}, \quad \Psi^{\dagger}_{\mathbf{p}} = \begin{pmatrix} c^{\dagger}_{\mathbf{p}\uparrow} & c_{-\mathbf{k}\downarrow} \end{pmatrix}, \tag{2.17}$$

known as the Nambu spinor. With this notation, the Hamiltonian can be written as

$$H = \sum_{\mathbf{p}} \Psi^{\dagger}_{\mathbf{p}} \begin{pmatrix} \xi_{\mathbf{p}} & -\Delta_{\mathbf{p}} \\ -\Delta^{*}_{\mathbf{p}} & -\xi_{\mathbf{p}} \end{pmatrix} \Psi_{\mathbf{p}}. \tag{2.18}$$

The Hamiltonian is almost diagonal, as the Nambu spinors with different momenta do not mix. We can then diagonalize these 2×2-blocks quite independent from each other. Diagonalizing the Hamiltonian with Bogoliubon γ-operators means that it can be written as

$$H = \sum_{\mathbf{p}\sigma} E_{\mathbf{p}} \gamma^{\dagger}_{\mathbf{p}\sigma} \gamma_{\mathbf{p}\sigma}, \tag{2.19}$$

with some yet undetermined dispersion $E_{\mathbf{p}}$. The γ-operators obey the anticommutation relation

$$\left\{ \gamma, \gamma^{\dagger} \right\} = \delta_{\mathbf{p}\mathbf{p}'}, \tag{2.20}$$

and they can be written as a linear mix of two time-reversed electron operators,

$$\begin{pmatrix} \gamma_{\mathbf{p}\uparrow} \\ \gamma^{\dagger}_{\mathbf{p}\downarrow} \end{pmatrix} = \begin{pmatrix} u_{\mathbf{p}} & -v_{\mathbf{p}} \\ v^{*}_{\mathbf{p}} & u^{*}_{\mathbf{p}} \end{pmatrix} \begin{pmatrix} c_{\mathbf{p}\uparrow} \\ c^{\dagger}_{-\mathbf{p}\downarrow} \end{pmatrix}. \tag{2.21}$$

The coefficients u and v can be determined by solving the Bogoliubov–de Gennes-equation

$$\begin{pmatrix} \xi_{\mathbf{p}} & \Delta_{\mathbf{p}} \\ \Delta^{*}_{\mathbf{p}} & -\xi_{\mathbf{p}} \end{pmatrix} \begin{pmatrix} u_{\mathbf{p}} \\ v_{\mathbf{p}} \end{pmatrix} = E_{\mathbf{p}} \begin{pmatrix} u_{\mathbf{p}} \\ v_{\mathbf{p}} \end{pmatrix}, \tag{2.22}$$

which has the structure of an eigenvalue equation. The dispersion can then be read from (2.22) as the determinant:

$$E_{\mathbf{p}} = \pm \sqrt{(\epsilon_{\mathbf{p}} - \mu)^2 + \Delta^2_{\mathbf{p}}}, \tag{2.23}$$

where the positive-energy solution corresponds to the states $\gamma_{\mathbf{p}}|\mathrm{G}\rangle$ and the negative-energy solution corresponds to the states $\gamma_{\mathbf{p}}^{\dagger}|\mathrm{G}\rangle$, where $|\mathrm{G}\rangle$ is the ground state of the superconducting phase.

Coefficients u and v can also be solved from the Bogoliubov-de Gennes equation. For the positive energy $E_{\mathbf{p}} > 0$, the solution is

$$u_{\mathbf{p}} = \frac{1}{\sqrt{2}}\sqrt{1 + \frac{\xi_{\mathbf{p}}}{E_{\mathbf{p}}}}, \quad \text{and} \quad v_{\mathbf{p}} = \frac{1}{\sqrt{2}}\sqrt{1 - \frac{\xi_{\mathbf{p}}}{E_{\mathbf{p}}}}. \tag{2.24}$$

When $\Delta \ll \xi_{\mathbf{p}}$, the magnitude of u is close to 1 and the magnitude of v is of the order of $\Delta_{\mathbf{p}}/E_{\mathbf{p}}$. For the negative-energy solution the roles of u and v are switched and their complex phases are different.

2.5 Self-consistency equation

In doing the mean field approximation we define Δ in Eq. (2.16) as a sum of some expectation values. Having diagonalized the Hamiltonian, we are now ready to evaluate them.

The expectation value written in the Bogoliubon operators is

$$\left\langle c_{\mathbf{p}\downarrow} c_{-\mathbf{p}\uparrow} \right\rangle = u_{\mathbf{p}} v_{\mathbf{p}} \left[2 \left\langle n_{\mathbf{p}}^{(\gamma)} \right\rangle - 1 \right], \tag{2.25}$$

where the γ-superscript signifies that we are considering the number operator which is composed with γ's and not with the electron number operator. Because the Hamiltonian is diagonal in γ's, the expectation value of their number operator is the Fermi-Dirac distribution. For negative energies the occupation is close to 1 and for positive energies

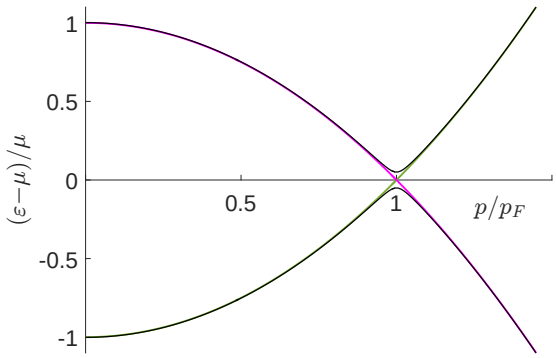

Figure 1. Two branches of the superconducting dispersion (2.23). Also pictured is the normal state electron dispersion (green line) and normal state hole dispersion (purple line). In the superconducting state, these two dispersions have hybridized and formed an avoided crossing of the width $2\Delta_0$ at the Fermi surface.

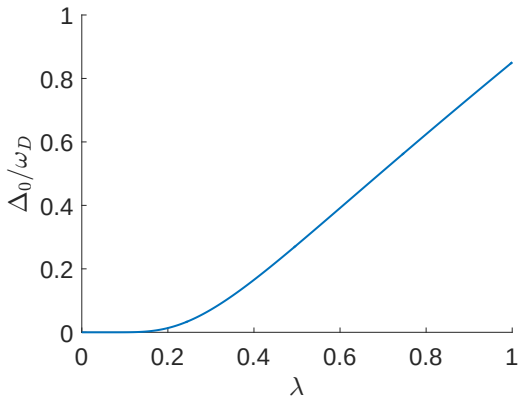

Figure 2. Magnitude of the order parameter Δ at zero temperature in the BCS theory. For small coupling λ superconductivity is exponentially suppressed, as expressed in (2.30). For $\lambda > 0.5$ the dependence on λ is linear.

it is close to 0:

$$\left\langle n_{\mathbf{p}}^{(\gamma)} \right\rangle = \frac{1}{e^{\beta E_{\mathbf{p}}^{\pm}} + 1}. \tag{2.26}$$

By plugging in the Fermi-Dirac distribution to Eq. (2.25), we get a hyperbolic tangent function. The product uv is

$$u_{\mathbf{p}}^{\pm} v_{\mathbf{p}}^{\pm} = \pm \frac{\Delta_{\mathbf{p}}}{2E_{\mathbf{p}}}. \tag{2.27}$$

In total, we have

$$\Delta_{\mathbf{p}} = -\sum_{\mathbf{p}'} \frac{V_{\mathbf{k}\mathbf{k}'} \Delta_{\mathbf{p}'}}{2E_{\mathbf{p}}} \tanh\left(\frac{\beta E_{\mathbf{p}}}{2}\right). \tag{2.28}$$

At zero temperature $\tanh(\beta E/2) = \operatorname{sgn}(E)$. By using the approximate interaction (2.12) and assuming a constant density of states at the Fermi surface, the order parameter is constant for $|\xi_{\mathbf{k}}| < \omega_D$ and the self-consistency simplifies at $T = 0$ to

$$\Delta = \frac{\lambda}{2} \int_{-\omega_{\mathrm{D}}}^{+\omega_{\mathrm{D}}} \mathrm{d}\xi \, \frac{\Delta}{\sqrt{\xi^2 + \Delta}}, \tag{2.29}$$

where $\lambda = N(0)V$ is a dimensionless parameter which describes the total strength of the interaction. $N(0)$ is the density of electron states at the Fermi level, which we get by changing the integration variable from momentum to energy in Eq. (2.28).

This can be solved as

$$\Delta = \frac{\omega_{\mathrm{D}}}{\sinh\left(1/\lambda\right)} \approx \begin{cases} 2\omega_{\mathrm{D}} \exp(-1/\lambda), & \text{for } \lambda \ll 1 \\ \lambda \omega_{\mathrm{D}}, & \text{for } \lambda \gg 1. \end{cases} \tag{2.30}$$

The function $\Delta(\lambda)$ is plotted in Fig. 2.

2.6 Transition temperature

The order parameter goes to zero at the transition temperature T_c. Just below the transition temperature, the self-consistency equation (2.28) is still valid, but $\Delta \approx 0$ and it can be written as

$$1 = \lambda \int_0^{\omega_\mathrm{D}} \frac{\mathrm{d}\xi}{\xi} \tanh\left(\frac{\xi}{2k_B T_c}\right). \tag{2.31}$$

This can be written as

$$\frac{1}{\lambda} = \int_0^{\frac{\omega_\mathrm{D}}{k_B T_c}} \frac{\mathrm{d}x}{x} \tanh\left(\frac{x}{2}\right) \tag{2.32}$$

Because $\tanh x \approx 1$ for large x, we can choose some large number M as a cutoff and approximate the integral above this number. This can be done, because $k_B T_c$ is of the same order as Δ, which we assume to be much smaller than ω_D.

$$\begin{aligned} \frac{1}{\lambda} &= \int_0^{M} \frac{\mathrm{d}x}{x} \tanh\left(\frac{x}{2}\right) + \int_M^{\frac{\omega_\mathrm{D}}{k_B T_c}} \frac{\mathrm{d}x}{x} \\ &= \int_0^{M} \frac{\mathrm{d}x}{x} \tanh\left(\frac{x}{2}\right) - \log(M) + \log\left(\frac{\omega_\mathrm{D}}{k_B T_c}\right) \\ &\approx\ 0.126 + \log\left(\frac{\omega_\mathrm{D}}{k_B T_c}\right), \end{aligned} \tag{2.33}$$

where, in the last step, M was taken to infinity. Exponentiating this, we find the critical temperature in the weak-coupling limit

$$k_B T_c = 1.13\, \omega_\mathrm{D} \exp\left(-\frac{1}{\lambda}\right), \tag{2.34}$$

which in terms of the zero temperature gap Δ_0 is

$$1.76 k_B T_c = \Delta_0. \tag{2.35}$$

In the case of very strong coupling $\lambda \gg 1$, the left hand side of Eq. (2.32) is small. Hence the upper limit of the integral also has to be small. We can then approximate $\tanh(x/2) \approx x/2$ and solve for T_c. We find

$$2k_B T_c = \lambda \omega_\mathrm{D} = \Delta_0 \tag{2.36}$$

This is however a dubious result, as we would expect the approximations made in the BCS theory not to be valid in the strong-coupling regime. Eliashberg theory provides corrections to this result, but we also expect that it should reduce to BCS limit in the weak-coupling regime.

3 Electron and phonon fields

To describe the phonon-mediated interaction in more detail than what is possible in the BCS theory, we consider the electron-phonon interaction from the field theoretical perspective. The Hamiltonian is the same as above, but for now the electron–electron Coulomb interaction is not considered,

$$\begin{aligned} H &= H_{\mathrm{e}} + H_{\mathrm{ph}} + H_{\mathrm{e\text{–}ph}} \\ &= \sum_{\mathbf{p}\sigma} \xi_{\mathbf{p}} c^\dagger_{\mathbf{p}\sigma} c_{\mathbf{p}\sigma} + \sum_{\mathbf{q}} \omega_{\mathbf{q}} b^\dagger_{\mathbf{q}} b_{\mathbf{q}} + \sum_{\mathbf{pq}\sigma} g_{\mathbf{q}} \left(b_{\mathbf{q}} + b^\dagger_{-\mathbf{q}} \right) c^\dagger_{\mathbf{p}+\mathbf{q},\sigma} c_{\mathbf{p}\sigma}. \end{aligned} \tag{3.1}$$

The electron-phonon interaction is formulated in terms of electron and phonon fields. The central concepts are Green's functions and self-energies. After we have formulated the electron-phonon interaction in normal state, the theory is generalized to the superconducting state. The field theoretical derivations are done with the equation-of-motion method, which allows for the self-consistency necessary to treat superconductivity. The derivation is done in a similar fashion as in the original paper by Éliashberg[8], but with some differences. For example, we use Matsubara formalism instead of the real-time formalism.

The central objects of interest in field theory are Green's functions. Green's functions originate from the theory of differential equations, where they are used to solve inhomogenous differential equations. Let us suppose we have a linear differential operator D_x with some boundary conditions. Green's function G for D_x then satisfies the equation

$$D_x G(x, y) = \delta(x - y),$$

where $\delta(x)$ is the Dirac delta function. Green's functions encountered in physics are Green's functions in this mathematical sense only in the case of non-interacting systems.

Even though the Green's functions can be treated as a purely mathematical tool, we can also attach physical meaning to them. As an example, consider the system at absolute zero on its ground state and the single-particle Green's function

$$G(x_1, x_2) = -i \left\langle 0 | T \hat{\psi}_\uparrow(x_1) \hat{\psi}^\dagger_\uparrow(x_2) | 0 \right\rangle, \tag{3.2}$$

where x contains both space and time coordinates: $x_i = (\mathbf{r}_i, t_i)$. If $t_1 > t_2$, then this Green's function can be interpreted as the propability amplitude for the state to evolve during time $t_1 - t_2$ from state $\hat{\psi}^\dagger_\uparrow(\mathbf{r}_2) |0\rangle$ to state $\hat{\psi}^\dagger_\uparrow(\mathbf{r}_1) |0\rangle$. At this point, there doesn't seem to be much of a connection between the mathematical and physical defitions of Green's function, but in the text below, we find that there is a common ground in which the two definitions coincide.

3.1 Matsubara formalism

Many-body perturbation theory comes in a few different flavours. The choice of formalism depends on what kind of observables one wants to calculate. In this thesis, we work with the Matsubara formalism, which allows us to calculate averages in thermal equilibrium. Dynamical processes are ruled out, as Matsubara formalism does not include time evolution in its contour[20]. To calculate time-dependent processes, a more versatile Keldysh formalism should be adopted. Here are mostly concerned about the phase transition from the normal to the superconducting state, so equilibrium considerations are sufficient and Matsubara formalism serves the purpose nicely.

Matsubara formalism is developed by utilizing the formal similarity between the unitary time-evolution operator $U = e^{iHt}$ and the thermal density operator $\rho = e^{\beta H}/Z$, where $Z = \operatorname{Tr} e^{\beta H}$. Using the similarity between ρ and U, we can define a 'time evolution' for the imaginary time

$$\hat{A}(\tau) = e^{H\tau}\hat{A}e^{-H\tau}. \tag{3.3}$$

The usual Heisenberg picture is obtained by setting $\tau{=}it$. For this reason Matsubara formalism is also known as imaginary-time formalism. We refer to parameter τ as time, even though it does not correspond to actual physical time.

Time-evolved annihilation and creation operators are

$$\begin{aligned} c_{\mathbf{p}\sigma}(\tau) &\equiv e^{H\tau}c_{\mathbf{p}\sigma}e^{-H\tau} \\ c^\dagger_{\mathbf{p}\sigma}(\tau) &\equiv e^{H\tau}c^\dagger_{\mathbf{p}\sigma}e^{-H\tau} \end{aligned} \tag{3.4}$$

Because this time-evolution is not unitary, $c^\dagger_{\mathbf{p}\sigma}(\tau) \neq [c_{\mathbf{p}\sigma}(\tau)]^\dagger$, except on the imaginary axis $\tau{=}it$.

Expectation values are calculated according to the usual rules of statistical mechanics,

$$\langle A\rangle = \operatorname{Tr}\rho\hat{A}, \tag{3.5}$$

where $\hat{A}$ is some operator. Usually we do not have to resort to this definition and explicitly calculate expectation values based on the density matrix, but it serves to motivate the definitions and boundary conditions for Green's functions.

Single-particle Green's operator is then defined as

$$G_\sigma(\mathbf{p},\tau,\tau') = -\left\langle Tc_{\mathbf{p}\sigma}(\tau)c^\dagger_{\mathbf{p}\sigma}(\tau')\right\rangle. \tag{3.6}$$

The sign of G is arbitrary, but here the normalization used corresponds to that used in Fetter and Walecka[21]. T is the time-ordering operator. It orders the operators in an increasing order from left to right with respect to τ. For two operators, this means that

$$TA(\tau)B(\tau') = \begin{cases} A(\tau)B(\tau'), & \tau < \tau' \\ B(\tau')A(\tau), & \tau > \tau' \end{cases} \tag{3.7}$$

Usually, hamiltonian H is time-independent, and G only depends on the difference $\tau - \tau'$, and not on the separate values of τ and τ'. We can then drop one time variable from G.

By using the cyclic property of the trace and the definition of the thermal density operator ρ, it can be shown that the fermionic propagator as defined in (3.6) is antiperiodic with the period β. This is known as Kubo-Martin-Schwinger (KMS) boundary condition,

$$G(\tau) = -G(\tau + \beta). \tag{3.8}$$

We can define Matsubara frequencies ω_n corresponding to time τ through Fourier transform. Because G is an antiperiodic function, the frequencies are discrete:

$$G(\tau) = \frac{1}{\beta} \sum_{n=-\infty}^{\infty} G(\omega_n) e^{-i\omega_n \tau}, \quad \text{with} \quad \omega_n = (2n+1)\pi/\beta. \tag{3.9}$$

In the inverse transformation the interval can be restricted to one period $[0, \beta]$ as implied by the KMS boundary condition:

$$G(\omega_n) = \int_0^\beta \mathrm{d}\tau \, G(\tau) e^{i\omega_n \tau} \tag{3.10}$$

A bosonic propagator, defined analogously to (3.6), but with operators obeying commutation instead of anticommutation rules, is a periodic function with period β:

$$D(\tau) = D(\tau + \beta). \tag{3.11}$$

This can be expressed in frequency space as

$$D(\tau) = \frac{1}{\beta} \sum_{n=-\infty}^{\infty} D(\omega_n) e^{-i\nu_n \tau}, \quad \text{with} \quad \nu_n = 2n\pi/\beta. \tag{3.12}$$

The important difference between the fermionic (3.9) and bosonic propagators (3.12) is that the fermionic propagator is defined at odd Matsubara frequencies ω_n and bosonic propagator at even Matsubara frequencies ν_n.

At zero temperature $\beta \to \infty$ and ω is a continuous variable. The frequency summations at the finite temperature can then be translated to zero temperature integrals by the substitution

$$\frac{1}{\beta} \sum_{n=-\infty}^{\infty} \to \int_{-\infty}^{\infty} \frac{\mathrm{d}\omega}{2\pi}. \tag{3.13}$$

Matsubara formalism simplifies many derivations by avoiding singularities on the real axis. This is especially handy when calculating solutions numerically, as we do not need to identify poles and do principal value integrations around them. However, the price to be paid is that the solutions we find are defined on the imaginary times and frequencies, when most of the physically meaningful information is on the real axis. Real and imaginary axes do intersect at $\tau = 0 = t$, so we can get static information directly from Matsubara

representation.

Translation from the imaginary propagator to the real-time retarded propagator can be obtained by finding an analytical function $G(z, \mathbf{p})$ which coincides with the Matsubara propagator at points $z = i\omega_n$ and which has no singularities at the upper half-plane $\mathrm{Im}\, z > 0$. This function is unique if we also require $G(\omega, \mathbf{p}) \to 0$, as $|\omega| \to \infty$.[22] If we already have an analytical expression for the imaginary-time Green's function, translation to the real time can be as simple as

$$i\omega_n \to \omega + i\eta,$$

where η is a positive infinitesimal.

In the interacting case, analytical expression is usually not be available, and we only know the Green's function in its discretized, numerical form. In such a case, the analytical continuation is a non-trivial task and there is no general method. In the Eliashberg case, this can be done either by Padé approximants[23], or by Marsiglio's method, which amounts to solving a set of non-linear integral equations[24].

3.2 Electron propagator in the normal state

I first demostrate the properties of Green's functions in the normal state. The generalization to the superconducting state is straightforward and the similarities and differences between the two states clearly stated.

Normal-state Green's function is already defined in (3.6), but I repeat the definition here.

$$G(\mathbf{p}, \tau) = -\left\langle T c_{\mathbf{p}\uparrow}(\tau) c^\dagger_{\mathbf{p}\uparrow}(0), \right\rangle \tag{3.14}$$

where, for definiteness, we have chosen the spin-up state. We are concerned with isotropic systems without magnetization, so spin-up and spin-down states are symmetric, $G_\uparrow = G_\downarrow$ and we do not need the label for spin. The time invariance of the Hamiltonian has also been used in eliminating the other time index τ' from the original definition.

Expanding the time-ordering operator with the Heaviside step function θ, we can write Green's function as

$$G(\mathbf{p}, \tau) = -\theta(\tau) \left\langle c_{\mathbf{p}\uparrow}(\tau) c^\dagger_{\mathbf{p}\uparrow}(0) \right\rangle + \theta(-\tau) \left\langle c^\dagger_{\mathbf{p}\uparrow}(0) c_{\mathbf{p}\uparrow}(\tau) \right\rangle . \tag{3.15}$$

By taking a time derivative of the above expression and reconstructing the time-ordering operator from the diffent step function parts, we get an equation of motion for the single-particle Green's function,

$$\frac{\mathrm{d}}{\mathrm{d}\tau} G(\mathbf{p}, t) = \delta(\tau) + \left\langle T \left\{ \frac{\mathrm{d}}{\mathrm{d}\tau} c_{\mathbf{p}\uparrow}(\tau) c^\dagger_{\mathbf{p}\uparrow}(0) \right\} \right\rangle , \tag{3.16}$$

where we use the anticommutation relation and the facts that the derivative of the θ-function is a Dirac delta function and $\langle 1 \rangle = 1$.

Derivative only acts on the first operator, since it is the only one with time dependence. Derivative of an operator A is given by the Heisenberg equation of motion

$$\frac{\mathrm{d}A_\mathrm{H}}{\mathrm{d}\tau} = [H,\, A_\mathrm{H}] + \frac{\partial A_\mathrm{H}}{\partial \tau}, \tag{3.17}$$

which is a consequence of the definition (3.3). The second term with a partial derivative would take into account explicit time dependence of the Hamiltonian, if we had any. To calculate the commutator in Eq. (3.17), the following identities are often useful:

$$[a_m^\dagger a_l, a_k] = -\delta_{mk} a_l, \tag{3.18}$$

$$[a_m^\dagger a_l, a_k^\dagger] = \delta_{kl} a_l^\dagger, \tag{3.19}$$

where a's and $a^\dagger$'s can be either bosonic or fermionic annihilation and creation operators.

In our case, for electrons with Hamiltonian (3.1), we have

$$\frac{\mathrm{d}}{\mathrm{d}\tau} c_{\mathbf{p}\uparrow}(\tau) = \xi_\mathbf{p} c_{\mathbf{p}\uparrow}(\tau) + \sum_\mathbf{q} g_\mathbf{q} \varphi_\mathbf{q}(\tau) c_{\mathbf{p}-\mathbf{q},\uparrow}(\tau). \tag{3.20}$$

The first term is due to commutation with H_e and the second with $H_\mathrm{e\text{–}p}$. Let us forget the electron-phonon interactions for a moment and determine Green's function G_0 which we would have if there were no interaction.

Substituting the relevant part from (3.20) to (3.16), we get

$$\frac{\mathrm{d}}{\mathrm{d}\tau} G_0(\mathbf{p}, \tau) = \delta(\tau) - \xi_\mathbf{p} \left\langle T c_{\mathbf{p}\uparrow}(\tau) c_{\mathbf{p}\uparrow}^\dagger(0) \right\rangle, \tag{3.21}$$

where the last term can be identified as the electron propagator. Moving that term to the left hand side, we get

$$\left(\frac{\mathrm{d}}{\mathrm{d}\tau} - \xi_\mathbf{p} \right) G_0(\mathbf{p}, \tau) = \delta(\tau), \tag{3.22}$$

from which we see that the non-interacting propagator G_0 is indeed a Green's function in a mathematical sense for the differential operator in parentheses. This fact does not extend to the interacting Green's functions.

This equation of motion can be solved algebraically in frequency space. Fourier transforming Eq. (3.22), we get

$$G_0(\mathbf{p}, i\omega_n) = \frac{1}{i\omega_n - \xi_\mathbf{p}}, \tag{3.23}$$

where the denominator is never zero, as ξ and ω_n are always real, and $\omega_n \neq 0$.

In the presence of interaction, Green's function becomes

$$\left(\frac{\mathrm{d}}{\mathrm{d}\tau} - \xi_\mathbf{p} \right) G(\mathbf{p}, t) = \delta(\tau) - \sum_\mathbf{q} g_\mathbf{q} \left\langle T \varphi_\mathbf{q}(\tau) c_{\mathbf{p}-\mathbf{q},\uparrow}(\tau) c_{\mathbf{p}\uparrow}^\dagger(0) \right\rangle \tag{3.24}$$

From this equation we see how the interactions are introduced to the system. To actually introduce them into our equations, we turn to the techniques of field theory and Feynman diagrams.

Much of the field theory is based on the classification of the Feynman diagrams into suitable classes which can then summed all at once. This is especially true in a self-consistent approach like the equation of motion method.

To get a perturbation expansion for G, it is useful to define a self-energy function Σ, which obeys the following equation in momentum-time space:

$$G(\mathbf{p},\tau) = G_0(\mathbf{p},\tau) + \int \mathrm{d}\tau_1\,\mathrm{d}\tau_2\, G_0(\mathbf{p},t_1)\Sigma(\mathbf{p},\tau_2-\tau_1)G(\mathbf{p},\tau-\tau_2) \tag{3.25}$$

Applying the differential operator from (3.22) to this, we get

$$\left(\frac{\mathrm{d}}{\mathrm{d}\tau} - \xi_{\mathbf{p}}\right) G(\mathbf{p},\tau) = \delta(\tau) + \int \mathrm{d}\tau'\,\Sigma(\mathbf{p},\tau')G(\mathbf{p},\tau-\tau') \tag{3.26}$$

Fourier transforming to frequency space, the differential operator becomes the inverse of the non-interacting propagator and we can solve for the interacting Green's function. The solution is

$$G(\mathbf{p},i\omega_n)^{-1} = G_0^{-1}(\mathbf{p},i\omega_n) - \Sigma(\mathbf{p},i\omega_n) \tag{3.27}$$

Which also tells us that the self-energy is the difference between the interacting and non-interacting Green's function, and as such represents the contribution from the interactions.

So far we have introduced the general framework in which we can incorporate the interactions, but the above text does not discuss the actual phonon-mediated interaction between electrons. It is introduced in the next section by formulating a specific form for the self-energy which can be inserted in Eq. (3.27).

3.3 Phonon-mediated interaction

We now formulate the phonon-mediated interaction between electrons in terms of the phonon field. At this point, the derivation is done quite formally. In Sec. 5, in order to justify some approximations, we take a more careful look into the properties of the interaction.

To describe the phonon-mediated interaction between electrons, we first need to find the propagator for the non-interacting phonons. To simplify the derivation of the phonon propagator, we define a phonon field operator

$$\varphi_{\mathbf{q}} = b_{\mathbf{q}} + b^{\dagger}_{-\mathbf{q}} \tag{3.28}$$

for which $\varphi^{\dagger}_{\mathbf{q}} = \varphi_{-\mathbf{q}}$. These operators commute with each other:

$$[\varphi_{\mathbf{q}}, \varphi_{\mathbf{q}'}] = 0.$$

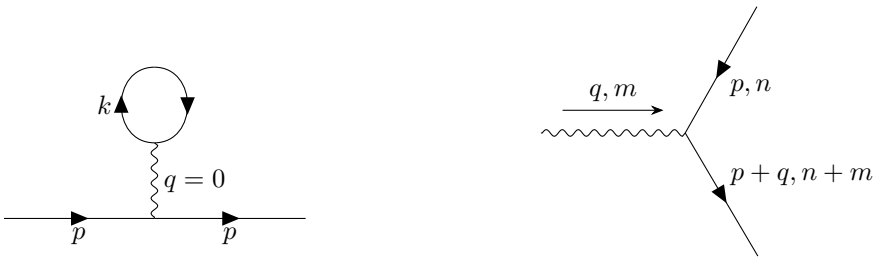

(a) Tadpole diagram **(b)** Bare vertex

Figure 3. Diagrams mentioned in the text

Thermal propagator for phonons is usually denoted by D and is defined similarly to (3.2)

$$D(\mathbf{q}, \tau) = -\left\langle T\varphi_{\mathbf{q}}(\tau)\varphi^{\dagger}_{\mathbf{q}}(0)\right\rangle. \tag{3.29}$$

Using the propagator defined with φ's instead of b's makes the Feynman rules for the theory somewhat simpler. If we would use the propagator $\left\langle Tb_{\mathbf{q}}b^{\dagger}_{\mathbf{q}}\right\rangle$, we would have to consider separately incoming and outgoing phonons. With D defined as above, only the transmitted four-momentum counts.

In this thesis, we do not consider phonon self-energy, but use the non-interacting propagator for phonons and only consider the interaction effects on electrons. The rationale behind this is that for real materials the phonon dispersion would usually be obtained from spectroscopic data, and if we use such an experimental dispersion, it already contains the contribution from the self-energy. We would be double-counting the diagrams if we would include it again.

For the non-interacting Hamiltonian, we notice that

$$\frac{\mathrm{d}^2\varphi_{\mathbf{q}}}{\mathrm{d}\tau^2} = \omega^2_{\mathbf{q}}\varphi_{\mathbf{q}}, \tag{3.30}$$

so in order to close the equations of motion, we have to take the second derivative:

$$\left(\frac{\mathrm{d}^2}{\mathrm{d}\tau^2} - \omega^2_{\mathbf{q}}\right) D(\mathbf{q}, \tau) = 2\omega_{\mathbf{q}}\delta(\tau). \tag{3.31}$$

The frequency form of the propagator is

$$D(\mathbf{q}, i\nu_n) = \frac{-2\omega_{\mathbf{q}}}{\omega^2_{\mathbf{q}} + \nu^2_n}, \tag{3.32}$$

where ν_n are now bosonic (even) Matsubara frequencies.

In terms of Feynman diagrams, electron self-energy can be defined as the sum of all the amputated diagrams in which one electron enters and one exits. Here 'amputated' means that we do not count diagrams in which the first or the last node is connected to a single propagator. We also only consider connected diagrams. Further, irreducible self-energy is defined as the sum of self-energy diagrams which cannot be cut into two by

removing one propagator. This is actually the self-energy that was defined in (3.25).

We also need to define a dressed vertex. A bare vertex of the electron-phonon interaction can be read from the Hamiltonian (3.1) and it gives a contribution of g to the diagrams. The bare vertex is shown in Fig. 3b. In the bare vertex, there are three branches: an incoming electron, an outgoing electron and a phonon. Dressed vertex Γ is then defined as the sum of all the (connected) diagrams which have one incoming electron, one outgoing electron and one entering phonon line. Its value $\Gamma(p, q)$ depends on the four-momentum p of the incoming electron and the four-momentum q of the phonon.

Because there is no zero-momentum phonon (it would amount to the translation of the whole crystal) there is also no tadpole diagram (fig. 3a) for phonons. It can then be seen that the complete electron self-energy can be expressed in one diagram:

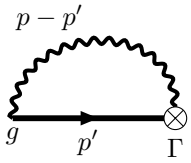

in which the thick lines denote dressed electron and phonon propagators and the crossed dot denotes the dressed vertex. This is known as the Dyson equation, and it can be written also as [25]

$$\Sigma(\mathbf{p}, i\omega_n) = T\sum_m \int \frac{\mathrm{d}^3\mathbf{p}'}{(2\pi)^3} gD(\mathbf{p}-\mathbf{p}', i\omega_n - i\omega_m) G(\mathbf{p}', i\omega_n) \Gamma(\mathbf{p}', i\omega_n; \mathbf{p}-p', i\omega_n - i\omega_m). \quad (3.33)$$

As mentioned above, we use the phonon propagator obtained in the previous section in place of the dressed propagator. Still, the relative simplicity of Dyson's equation is deceiving, as the vertex function is actually a very complex object. Luckily, in the electron-phonon case, it can be approximated with good accuracy by the bare vertex. The justification for this comes from Migdal's theorem[7] which is discussed in the next section. After that approximation, Dyson's equation is

$$\Sigma(\mathbf{p}, i\omega_n) = T\sum_m \int \frac{\mathrm{d}^3\mathbf{p}'}{(2\pi)^3} g^2 D(\mathbf{p}-\mathbf{p}', i\omega_n - i\omega_m) G(\mathbf{p}', i\omega_n). \quad (3.34)$$

From the point of view of electrons, phonons act as mediators of an effective force. The 'potential' associated with this force is

$$g^2 D(\mathbf{q}, \omega) = -\frac{2g^2\omega_{\mathbf{q}}}{\omega_{\mathbf{q}}^2 - \omega^2}, \quad (3.35)$$

and we can see that the interaction is attractive (has a negative sign) for frequencies $|\omega| < \omega_{\mathbf{q}}$. Of course this is not an ordinary potential, because it depends on the frequency ω, which has a meaning only in the context of Green's functions.

(a) **(b)**

Figure 4. Ladder diagrams

3.4 Migdal's adiabatic theorem

There is a theorem by Migdal[7] according to which we can with good a accuracy replace the dressed vertex Γ by the bare g in the usual metallic systems where the phonon and electron energy scales are separate: $\omega_D \ll \varepsilon_F$. The justification is based on the argument that the most important class of diagrams contributing to the vertex are so-called ladder diagrams, which are pictured in Fig. 4. By calculating the relative contribution to the dressed vertex from the first ladder diagram, it can be seen that it is usually of the order

$$\mathcal{O}(\lambda\frac{\omega_D}{\varepsilon_F}),$$

where λ is the dimensionless coupling parameter corresponding to the BCS interaction strength,

$$\lambda = \frac{2g^2N(0)}{\omega_D}. \tag{3.36}$$

Ladder diagrams can be defined recursively, so the contribution from the second order ladder is

$$\mathcal{O}(\left(\lambda\frac{\omega_D}{\varepsilon_F}\right)^2),$$

and so on for the following orders. This means that the expansion parameter in our field theory is not λ, but λ times the ratio between typical phonon and electron energies, which is typically of the order $\sim 1/100$. This ratio is also often written as $\sqrt{m/M}$, where m and M are the mass of the electron and the nucleus, respectively. Migdal's theorem can thus be considered as a many-body perturbation theory analogue to the Born-Oppenheimer approximation.

Migdal's theorem is valid in metals, but in flat-band systems the validity has to be verified separately, as the energy scales of phonons and electrons might be of the same order or ordered differently with respect to each other.

4 Eliashberg theory for electron-phonon interaction

We are now ready to move on to discuss superconductivity. In the normal state, normal propagator (3.2) is all we need to describe electrons. This is because other expectation values of combinations of annihilation and creation operators vanish. But as we learn from the BCS model, in the superconducting phase we also have the non-vanishing anomalous expectation value. In field theory, the non-vanishing expectation value corresponds to a non-vanishing propagator. We can define two anomalous propagators

$$F(\mathbf{p},\tau) = -\left\langle Tc_{\mathbf{p}\uparrow}(\tau)c_{-\mathbf{p}\downarrow}(0)\right\rangle \tag{4.1}$$

$$\bar{F}(\mathbf{p},\tau) = -\left\langle Tc^{\dagger}_{-\mathbf{p}\downarrow}(\tau)c^{\dagger}_{\mathbf{p}\uparrow}(0)\right\rangle. \tag{4.2}$$

These function are even in time,

$$F(\mathbf{p},\tau) = F(\mathbf{p},-\tau) \quad \text{and} \quad \bar{F}(\mathbf{p},\tau) = \bar{F}(\mathbf{p},-\tau), \tag{4.3}$$

which means that they are also even in frequency,

$$F(\mathbf{p},i\omega_n) = F(\mathbf{p},-i\omega_n) \quad \text{and} \quad \bar{F}(\mathbf{p},i\omega_n) = \bar{F}(\mathbf{p},-i\omega_n). \tag{4.4}$$

If $F(\mathbf{p},i\omega_n)$ is chosen to be real (in isolated superconductor this is possible by gauge freedom), then it can also be shown by taking a complex conjugate of Eq. (4.1) that F and $\bar{F}$ coincide,

$$\bar{F}(\mathbf{p},i\omega_n) = F(\mathbf{p},i\omega_n). \tag{4.5}$$

The equation of motion for F is

$$\left(\frac{\mathrm{d}}{\mathrm{d}\tau} - \xi_{\mathbf{p}}\right) F(\mathbf{p},t) = -\sum_{\mathbf{q}} g_{\mathbf{q}} \left\langle T\varphi_{\mathbf{q}}(\tau)c_{\mathbf{p}-\mathbf{q}\uparrow}(\tau)c_{-\mathbf{p}\downarrow}(0)\right\rangle \tag{4.6}$$

In this case, the annihilation operators always anti-commute, so there is no delta function in the equation of motion, and the non-interacting F vanishes. As it should, because there is no superconductivity without interactions.

We also need the time-reversed propagator

$$\bar{G}(\mathbf{p},i\omega_n) = -\left\langle Tc^{\dagger}_{-\mathbf{p}\downarrow}(\tau)c_{-\mathbf{p}\downarrow}(0)\right\rangle \tag{4.7}$$

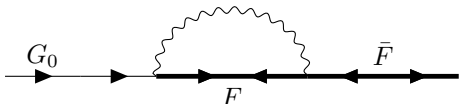

Figure 5. Diagram which contributes to G and modifies the Dyson equation. With equal number of F's and $\bar{F}$'s the electron number is conserved.

As the name suggests, $\bar{G}(\tau) = G(-\tau)$. For the frequency representation this implies

$$\begin{aligned}\bar{G}(\mathbf{p}, i\omega_n) &= \int_0^\beta \mathrm{d}\tau\, e^{i\omega_n\tau} G(-\tau) = \int_{-\beta}^0 \mathrm{d}\tau\, e^{-i\omega_n\tau} G(\tau) \\ &= \int_0^\beta \mathrm{d}\tau\, e^{-i\omega_n\tau} G(\tau+\beta) = -\int_0^\beta \mathrm{d}\tau\, e^{-i\omega_n\tau} G(\tau) \\ &= -G(\mathbf{p}, -i\omega_n),\end{aligned} \tag{4.8}$$

where the last step follows from the KMS boundary condition (3.8).

In the presence of the anomalous propagator, Dyson's equation (3.34) ceases to be valid. The reason for this is that if we define G to include all the diagrams in which one electron enters and one exits, then we get contributions from F as well, for example the diagram shown in Fig. 5. The easiest way to generalize Dyson's equation for a superconductor is to write everything in the Nambu basis.

4.1 Collecting time-reversed states in a Nambu spinor

In the above derivation of the BCS theory the Nambu trick helps us to diagonalize the Hamiltonian. Here it is useful because in the Nambu basis the Feynman rules for the normal metal can be translated into Feynman rules for the superconductor with minor modifications. In particular, the similarity between the Feynman rules means that the Dyson equation also has a form analogous to (3.34).

The Nambu spinors are defined as above,

$$\Psi_{\mathbf{p}} = \begin{pmatrix} c_{\mathbf{p}\uparrow} \\ c^\dagger_{-\mathbf{p}\downarrow} \end{pmatrix}, \quad \Psi^\dagger_{\mathbf{p}} = \begin{pmatrix} c^\dagger_{\mathbf{p}\uparrow} & c_{-\mathbf{p}\downarrow} \end{pmatrix}. \tag{4.9}$$

Pauli matrices in Nambu space are written with τ to distinguish them from Pauli matrices operating in spin space commonly denoted with σ's. They are

$$\mathbb{1} = \begin{pmatrix} 1 & 0 \\ 0 & 1 \end{pmatrix}, \quad \tau_1 = \begin{pmatrix} 0 & 1 \\ 1 & 0 \end{pmatrix}, \quad \tau_2 = \begin{pmatrix} 0 & -i \\ i & 0 \end{pmatrix}, \quad \tau_3 = \begin{pmatrix} 1 & 0 \\ 0 & -1 \end{pmatrix}. \tag{4.10}$$

Hamiltonian (3.1) can be written in terms of diagonal Pauli matrices $\mathbb{1}$ and τ_3:

$$\begin{aligned} H_{\mathrm{e}} &= \sum_{\mathbf{p}} \xi_{\mathbf{p}} \Psi^\dagger_{\mathbf{p}} \tau_3 \Psi_{\mathbf{p}} = \sum_{\mathbf{p}} \Psi^\dagger_{\mathbf{p}} \begin{pmatrix} \xi_{\mathbf{p}} & 0 \\ 0 & -\xi_{\mathbf{p}} \end{pmatrix} \Psi_{\mathbf{p}}, \\ H_{\mathrm{e\text{–}p}} &= \sum_{\mathbf{pq}} g_{\mathbf{q}} \varphi_{\mathbf{q}} \Psi_{\mathbf{p}+\mathbf{q}} \tau_3 \Psi_{\mathbf{p}}, \end{aligned} \tag{4.11}$$

and the non-interacting phonon part is unmodified.

We can then define a matrix propagator, which collects in one matrix both the normal and anomalous propagators as defined in the previous section,

$$\begin{aligned} \mathbf{G}(\mathbf{p},\tau) &= -\left\langle T\Psi_{\mathbf{p}}(\tau)\Psi^\dagger_{\mathbf{p}}(0)\right\rangle \equiv \begin{pmatrix} G(\mathbf{p},\tau) & F(\mathbf{p},\tau) \\ \bar{F}(\mathbf{p},\tau) & \bar{G}(\mathbf{p},\tau) \end{pmatrix} \\ &= -\begin{pmatrix} \langle T c_{\mathbf{p}\uparrow}(\tau) c^\dagger_{\mathbf{p}\uparrow}(0)\rangle & \langle T c_{\mathbf{p}\uparrow}(\tau) c_{-\mathbf{p}\downarrow}(0)\rangle \\ \langle T c^\dagger_{-\mathbf{p}\downarrow}(\tau) c^\dagger_{\mathbf{p}\uparrow}(0)\rangle & \langle T c^\dagger_{-\mathbf{p}\downarrow}(\tau) c_{-\mathbf{p}\downarrow}(0)\rangle \end{pmatrix}. \end{aligned} \tag{4.12}$$

In frequency space, this is

$$\mathbf{G}(\mathbf{p},\omega) = \begin{pmatrix} G(\mathbf{p},\omega) & F(\mathbf{p},\omega) \\ F(\mathbf{p},\omega) & -G(\mathbf{p},-\omega) \end{pmatrix}, \tag{4.13}$$

where we take the symmetries (4.5) and (4.8) into account.

4.2 Nambu equation of motion and Dyson's equation

The non-interacting propagator can be determined with the equation of motion method from the Hamiltonian (4.11)

$$\mathbf{G}_0(\mathbf{p},\omega) = [\omega\mathbb{1} - \xi_{\mathbf{p}}\tau_3]^{-1}. \tag{4.14}$$

For the interacting propagator, we just add the self-energy,

$$\mathbf{G}(\mathbf{p},\omega) = \left[\mathbf{G}_0^{-1}(\mathbf{p},\omega) - \mathbf{\Sigma}(\mathbf{p},\omega)\right]^{-1}. \tag{4.15}$$

The irreducible self-energy $\mathbf{\Sigma}$ is defined through the Dyson's equation [9]

$$\mathbf{\Sigma}(\mathbf{p}, i\omega_n) = T\sum_m \int \frac{\mathrm{d}^3\mathbf{p}'}{(2\pi)^3} g^2 D(\mathbf{p}-\mathbf{p}', i\omega_n - \omega_m)\tau_3 \mathbf{G}(\mathbf{p}', i\omega_m)\tau_3, \tag{4.16}$$

where we again use Migdal's theorem and approximate the vertex with its bare value as in the normal state. The effect of sandwiching $\tau_3\mathbf{G}\tau_3$ is just to switch the signs on the off-diagonal terms.

There is a small difference between the phonon propagator in the normal state and in the phonon propagator in the superconducting state, which comes from contribution of the anomalous propagator to the phonon self-energy. This contribution only affects phonons

with energy comparable to Δ. In particular, in the superconducting state, phonons with energy less than 2Δ are unable to decay into electron-hole pair so that their lifetime becomes infinite. For phonons with energies just above 2Δ, the decay rate is enhanced and the lifetime diminished.[26] Because only a small fraction of the phonons is affected by this effect, with little weight in the integral of Eq. (4.16), the effective interaction between the electrons is not significantly altered, and we can use the same phonon propagator D in the superconducting state as in the normal state.

The equations above have simple forms in Nambu space. However, to obtain expressions for the separate components, we write them in a matrix form. First we divide the self-energy into diagonal (normal) and off-diagonal (anomalous) components:

$$\mathbf{\Sigma}(\mathbf{p}, i\omega_n) = \begin{pmatrix} \Sigma(\mathbf{p}, \omega) & \phi(\mathbf{p}, \omega) \\ \phi^*(\mathbf{p}, \omega) & \Sigma(\mathbf{p}, -\omega) \end{pmatrix}. \tag{4.17}$$

With this notation, we can calculate the inverse matrix in (4.15). Suppressing the momentum index, the result is

$$\mathbf{G}(i\omega_n) = \frac{1}{\Omega(\mathbf{p}, i\omega_n)} \begin{pmatrix} G_0^{-1}(-i\omega_n) + \Sigma(-i\omega_n) & -\phi(i\omega_n) \\ -\phi^*(i\omega_n) & G_0^{-1}(i\omega_n) + \Sigma(i\omega_n) \end{pmatrix}, \tag{4.18}$$

where Ω is the determinant of the inverted matrix:

$$\Omega(i\omega_n) = \Big[i\omega_n - \xi_{\mathbf{p}} - \Sigma(i\omega_n)\Big] \times \Big[i\omega_n + \xi_{\mathbf{p}} + \Sigma(-i\omega_n)\Big] - |\phi(i\omega_n)|^2. \tag{4.19}$$

Note that Ω is an even function of frequency,

$$\Omega(i\omega_n) = \Omega(-i\omega_n). \tag{4.20}$$

From Dyson's equation (4.16) we have an equation for $\mathbf{\Sigma}$ in terms of $\mathbf{G}$, and from the equation of motion (4.18) we have an equation for $\mathbf{G}$ in terms of $\mathbf{\Sigma}$. The loop can be closed by substituting $\mathbf{G}$ from the latter equation into the former equation. We thus obtain a self-consistency equation for the self-energy. Before writing down that equation, it is useful to divide the self-energy a bit further into different components in Nambu basis. This is done in the next section.

4.3 Eliashberg equations

Divide the diagonal part of the self-energy into odd and even frequency components,

$$\Sigma(i\omega_n) - \Sigma(-i\omega_n) = i[1 - Z(i\omega_n)]\omega_n, \tag{4.21}$$

$$\Sigma(i\omega_n) + \Sigma(-i\omega_n) = \chi(i\omega_n). \tag{4.22}$$

Defined this way, both Z and χ are even functions in frequency. Note that with no interactions and no self-energy, Z=1. Also, because of the symmetries in Green's function

described in Eq. (4.8), we can associate Z with the matrix $\mathbb{1}$ and χ with τ_3. ϕ can also be divided into a real and complex parts ϕ_1 and ϕ_2, corresponding to matrices τ_1 and τ_2, respectively. The self-energy can then be written as

$$\mathbf{\Sigma} = i[1 - Z]\omega_n \mathbb{1} + \phi_1\tau_1 + \phi_2\tau_2 + \chi\tau_3. \tag{4.23}$$

Pauli matrices and $\mathbb{1}$ form a complete basis for these hermitian 2×2 matrices, so the expression above is completely general in a spin-symmetric Nambu space. We already chose ϕ to be real, so $\phi_2 = 0$ and we do not have to consider the τ_2 component.

The Nambu propagator is then

$$\mathbf{G}(\mathbf{p}, i\omega_n) = -\frac{i\omega_n Z(\mathbf{p}, i\omega_n)\mathbb{1} + [\xi_{\mathbf{p}} + \chi(\mathbf{p}, i\omega_n)]\,\tau_3 + \phi(\mathbf{p}, i\omega_n)\tau_1}{\Omega(\mathbf{p}, i\omega_n)}, \tag{4.24}$$

where

$$\Omega(\mathbf{p}, i\omega_n) = [Z(\mathbf{p}, i\omega_n)\omega_n]^2 + [\xi_{\mathbf{p}} + \chi(\mathbf{p}, i\omega_n)]^2 + [\phi(\mathbf{p}, i\omega_n)]^2. \tag{4.25}$$

Substituting now the $\mathbf{G}$ to Dyson's equation (4.16), we obtain the Eliashberg equations for the different self-energy components, [26]

$$\phi(\mathbf{p}, i\omega_n) = -\int \frac{\mathrm{d}^3\mathbf{p}'}{(2\pi)^3}\frac{1}{\beta}\sum_m g^2_{\mathbf{p}-\mathbf{p}'} D(\mathbf{p}-\mathbf{p}', i\omega_n - i\omega_m)\frac{\phi(\mathbf{p}', i\omega_m)}{\Omega(\mathbf{p}', i\omega_m)} \tag{4.26}$$

$$Z(\mathbf{p}, i\omega_n) = 1 - \int \frac{\mathrm{d}^3\mathbf{p}'}{(2\pi)^3}\frac{1}{\beta}\sum_m g^2_{\mathbf{p}-\mathbf{p}'} D(\mathbf{p}-\mathbf{p}', i\omega_n - i\omega_m)\frac{\omega_m}{\omega_n}\frac{Z(\mathbf{p}', i\omega_m)}{\Omega(\mathbf{p}', i\omega_m)} \tag{4.27}$$

$$\chi(\mathbf{p}, i\omega_n) = +\int \frac{\mathrm{d}^3\mathbf{p}'}{(2\pi)^3}\frac{1}{\beta}\sum_m g^2_{\mathbf{p}-\mathbf{p}'} D(\mathbf{p}-\mathbf{p}', i\omega_n - i\omega_m)\frac{\xi_{\mathbf{p}'} + \chi(\mathbf{p}', i\omega_m)}{\Omega(\mathbf{p}', i\omega_m)} \tag{4.28}$$

These different components only couple through the common denominator Ω. The equation for ϕ always has a trivial solution $\phi = 0$, which corresponds to the normal state. Z and χ are generally also present in the normal state, and are only slightly altered by the transition to the superconducting state.

The connection between the BCS energy gap Δ and the anomalous self-energy ϕ can be established by considering the quasiparticle spectrum from the poles of the propagator for which $\Omega = 0$. This can be naturally done in real frequencies, not in the Matsubara formalism. Define Δ as the energy gap, so that it corresponds to the the lowest energy excitation. This excitation occurs at the fermi surface $|\mathbf{p}| = p_F$. Δ satisfies the equation

$$\Delta = \frac{\phi(p_F, \Delta)}{Z(p_F, \Delta)} \approx \frac{\phi(p_F, 0)}{Z(p_F, 0)}, \tag{4.29}$$

where the approximation is valid if $\Delta \ll \omega_D$, because then $Z(p_F, \Delta) \approx Z(p_F, 0)$ and $\phi(p_F, \Delta) \approx \phi(p_F, 0)$.

Z-component of the self-energy can be interpreted in metals as the relative change in the Fermi velocity due to electron–phonon interaction. This can be seen by considering the normal state, and an electron on its mass shell with energy E_p, so that $\omega = E_p$

(assuming spherically symmetric Fermi surface). Then the dispersion relation modified by the interactions can be determined self-consistently from[27]

$$E_p = \varepsilon_p + \Sigma(p, E_p) = \varepsilon_p + (1 - Z(p, E_p))E_p, \tag{4.30}$$

where χ is neglected, as in metals it is usually small compared to other energies. Taking the derivative with respect to p at the Fermi momentum p_F on both sides gives

$$\left.\frac{\mathrm{d}E_p}{\mathrm{d}p}\right|_F = v_F + \left(\frac{\partial Z}{\partial p} + \left.\frac{\partial Z}{\partial \omega}\right|_{\omega=0} \frac{\partial E_p}{\partial p}\right) E_{p_F} + (1 - Z(p_F, 0))\left.\frac{\mathrm{d}E_p}{\mathrm{d}p}\right|_F, \tag{4.31}$$

where the derivative of Z was decomposed into a sum of partial derivatives. As the momentum dependence of the electron-phonon interaction is usually weak, the partial derivative of Z with respect to p is small. Also, the partial derivative with respect to ω vanishes at the Fermi level ($\omega = 0$), because Z is even in frequency. Thus, we have

$$v_F^* = \frac{\mathrm{d}E_p}{\mathrm{d}p} = \frac{v_F}{Z(p_F, 0)}, \tag{4.32}$$

which can be interpreted as the effective Fermi velocity in the presence of electron–phonon coupling. By reducing the Eliashberg equations to the BCS limit, it is seen below that the presence of Z reduces the strength of the effective interaction and opposes superconductivity.

4.4 Equation for the chemical potential

We get the electron density from the diagonal component of Nambu Green's function,[26]

$$\begin{aligned} n_{\mathbf{p}\uparrow} - 1 &= -\left\langle c_{\mathbf{p}\uparrow} c_{\mathbf{p}\uparrow}^\dagger \right\rangle = G(\mathbf{p}, \tau{=}0) \\ &= \lim_{\tau \to 0+} T \sum_n G(\mathbf{p}, i\omega_n) e^{i\omega_n \tau} \end{aligned}$$

The total number density is fixed, so this creates an equation for the chemical potential μ:

$$n = 1 - 2T \sum_{n,p} \frac{\varepsilon_{\mathbf{p}} - \mu + \chi_n}{[Z_n \omega_n]^2 + [\varepsilon_{\mathbf{p}} - \mu + \chi_n]^2 + \phi_n^2}. \tag{4.33}$$

This equation would also be present even if there were no interactions. At a finite temperature, the occupation of states is described by the Fermi-Dirac distribution, and if the density of states is unequally distributed below and above $\mu(T{=}0)$, the potential has to be shifted to keep the electron number fixed as the temperature is raised. The appearance of the self-energy functions in this relation just reflects the fact that they alter the density of states.

If the density of states can be considered symmetric above and below $\mu(T{=}0)$, then the equation is trivially satisfied, and the potential is constant in temperature. Most of the models considered in this thesis are symmetric this way, the sole exception being the

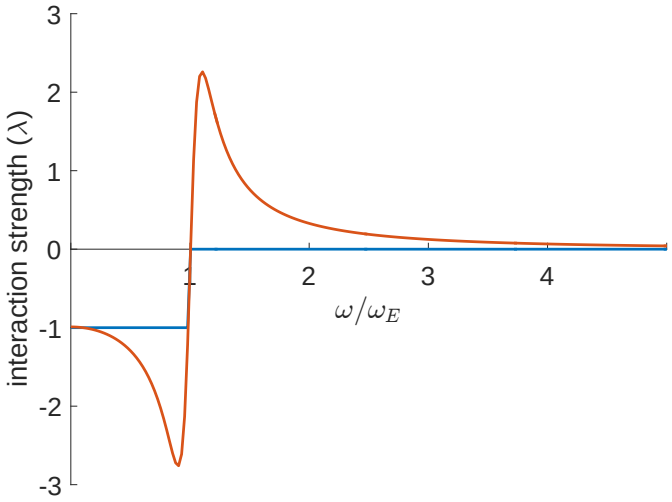

Figure 6. Effective interaction strength for Einstein spectrum (red) and the BCS step function approximation (blue). A small positive imaginary part has been added to the denominator of the propagator to round the divergence at $\omega = \omega_E$.

dispersion defined before Eq. (5.14).

4.5 BCS limit

BCS theory can be obtained from the Eliashberg equations (4.26–4.28) by approximating the phonon propagator with its static value up to the cutoff ω_E. In real frequencies, the propagator for Einstein phonons is

$$D(\mathbf{q},\omega) = \frac{-2\omega_E}{\omega_E^2 - (\omega + i\delta)^2}, \tag{4.34}$$

where δ is an infinitesimal quantity. The propagator has a negative sign for $\omega < \omega_E$ as shown in Fig. 6. Taking this as the most important feature of the interaction, it can be approximated by

$$\begin{aligned} D(\mathbf{q},\omega) &\approx D(\mathbf{q},0)\ \Theta(|\omega| - \omega_E) \\ &\approx D(\mathbf{q},0)\ \Theta(|\varepsilon_{\mathbf{k}+\mathbf{q}} - \varepsilon_{\mathbf{k}}| - \omega_E) \\ &= -\lambda\Theta(|\varepsilon_{\mathbf{k}+\mathbf{q}} - \varepsilon_{\mathbf{k}}| - \omega_E). \end{aligned} \tag{4.35}$$

With the cutoff moved from the frequency to the momentum space, the Matsubara sums can be done with the identity

$$\frac{1}{\beta}\sum_m \frac{1}{\omega_m^2 + E^2} = \frac{1}{2E}\tanh\left(\frac{\beta E}{2}\right). \tag{4.36}$$

For weak coupling $Z(\omega = 0) \approx 1 + \lambda$ and $\phi \approx \Delta/(1 + \lambda)$, so after approximating the

density of states with a constant $N(0)$, the Eliashberg equation for ϕ becomes

$$\Delta(\varepsilon) = \frac{\lambda N(0)}{1+\lambda} \int_{-\omega_E}^{+\omega_E} \mathrm{d}\varepsilon' \, \frac{\Delta(\varepsilon')}{2\sqrt{\varepsilon'^2 + \Delta(\varepsilon')^2}} \tanh\left(\frac{\sqrt{\varepsilon'^2 + \Delta(\varepsilon')^2}}{2T}\right), \tag{4.37}$$

This has the same form as the finite-temperature BCS equation (2.28), with a slight reduction to λ coming from the self-energy function $Z = 1 + \lambda$.

5 Eliashberg equations in metals

By using $g^2_{\mathbf{q}} D(\mathbf{q}, \nu_n)$ as the interaction kernel in Eqs. (4.26–4.28), we are considering scatterings from momentum state $\mathbf{p}$ to another momentum state $\mathbf{p}'$. In this work we limit the discussion on isotropic superconductivity, and therefore it is enough to express our integrals as scatterings between different energies $\xi_{\mathbf{p}}$ and $\xi_{\mathbf{p}'}$.

To achieve this, we first write the 3D momentum integral that appears in Eqs. (4.26–4.28) as an integral over energy ξ and transferred momentum q. In spherical coordinates, the original integral over $\mathbf{p}'$ is

$$\int \frac{\mathrm{d}^3}{(2\pi)^3}\mathbf{p}' = \frac{1}{4\pi^2}\int_0^\infty \mathrm{d}p'\, p'^2 \int_{-1}^{+1} \mathrm{d}u\,, \quad \text{with} \quad u = \cos\theta, \tag{5.1}$$

and z-axis from which the angles are measured is chosen along $\mathbf{p}$.

Let's change $q = |\mathbf{p} - \mathbf{p}'|$ as the integration variable instead of u. The Jacobian is simply

$$J = \left|\frac{\partial u}{\partial q}\right| = \frac{q}{pp'},$$

and the integral becomes

$$\int \frac{\mathrm{d}^3\mathbf{p}'}{(2\pi)^3} = \frac{1}{4\pi^2 p}\int \mathrm{d}p'\, p' \int_{|p-p'|}^{p+p'} \mathrm{d}q\, q. \tag{5.2}$$

The q-integration limits are complicated. However, because the integral appears in the context of electron-phonon interactions, we can do some approximations.

First of all, we choose $\mathbf{p}$ from the Fermi surface. We then notice that the largest contribution to Eqs. (4.26–4.28) comes from the region near the Fermi surface. For this reason $p \approx p_F$ and $p' \approx p_F$ and we can simplify the q-integral limits:[28]

$$\begin{aligned}\int \frac{\mathrm{d}^3\mathbf{p}'}{(2\pi)^3} &\approx \frac{1}{4\pi^2 p_F}\int_0^\infty \mathrm{d}p'\, p' \int_0^{2p_F} \mathrm{d}q\, q \\ &= N(0)\int \mathrm{d}\xi \int_0^{2p_F} \mathrm{d}q\, q.\end{aligned} \tag{5.3}$$

The integrals in Eqs. (4.26–4.28) which we are considering have a common part with a phonon propagator, which can be written as

$$\int \frac{\mathrm{d}^3\mathbf{p}'}{(2\pi)^3} g^2_{\mathbf{p}-\mathbf{p}'} D(\mathbf{p}-\mathbf{p}', z) \approx \int \mathrm{d}\xi \int_0^{2p_F} \mathrm{d}q\, \frac{q}{2p_F^2} \int \mathrm{d}\nu\, \frac{-2\nu g^2 N(0)}{\nu^2 + z^2}\delta(\nu - \omega_q), \tag{5.4}$$

where the approximation was to confine the $\mathbf{p}$ and $\mathbf{p}'$ to the Fermi surface. We also wrote

the phonon spectrum in terms of energies. Next we average the interaction over q's by replacing $\delta(\omega_q - \nu)$ with the $F(\nu)$, which is the phonon density of states at energy ν.

It is then conventional to define the Eliashberg function[29]

$$\alpha^2 F(\nu) = N(0) g^2 F(\nu), \tag{5.5}$$

where the combination $\alpha^2 F$ is understood as one symbol. The average interaction at the Fermi surface is then described by the interaction kernel

$$\lambda(z) = \int_0^\infty \mathrm{d}\nu \, \frac{2\nu \alpha^2 F(\nu)}{z^2 - \nu^2}, \tag{5.6}$$

which depends only on Matsubara indices, not on the momenta. This function replaces the propagator $g^2 D$ in the Eliashberg equations, as we see in the next section. Writing the interaction with the Eliashberg function is also useful because it connects the electron-phonon interaction to density of phonon states, which can be experimentally determined.

5.1 Interaction kernels for Einstein and Debye phonons

For the Einstein phonons, all the phonons have the same energy and the density of states is a Dirac delta function at energy ω_E. The interaction kernel is

$$\lambda_E(z) = \frac{2g^2 N(0)\omega_E}{z^2 - \omega_E^2} = \frac{\lambda \omega_E^2}{z^2 - \omega_E^2}, \quad \text{with} \quad \lambda = \frac{2g^2 N(0)}{\omega_E}. \tag{5.7}$$

In this simple case, $\lambda(z)$ corresponds exactly to $g^2 D(z) N(0)$. λ, defined as above is dimensionless, and is the natural choice to describe the strength of the effective interaction.

Debye phonons have the dispersion $\omega_{\mathbf{q}} = cq$ for $q < q_M$, where c is the speed of sound in the material and q_M is a momentum cutoff defined by $\omega_D = c q_M$, where ω_D is the Debye energy of the material. Density of states is defined through the relation between energy and momentum integrals:

$$\int_0^\infty \mathrm{d}\nu \, F(\nu) = \int \frac{\mathrm{d}^3\mathbf{q}}{(2\pi)^3} = \frac{1}{2\pi^2} \int_0^{q_M} \mathrm{d}q \, q^2 = \frac{1}{2\pi^2 c^3} \int_0^{\omega_D} \mathrm{d}\nu \, \nu^2, \tag{5.8}$$

from which we find the density of states

$$F(\nu) = \frac{\nu^2}{2\pi^2 c^3} \Theta(\nu - \omega_D). \tag{5.9}$$

For Debye phonons in a simple electron gas model, after taking screening into account, the electron-phonon coupling is[30]

$$g_{\mathbf{q}} = \frac{Ze^2}{\epsilon_0} \frac{q}{q^2 + k_s^2} \sqrt{\frac{N}{2M\omega_q}}, \tag{5.10}$$

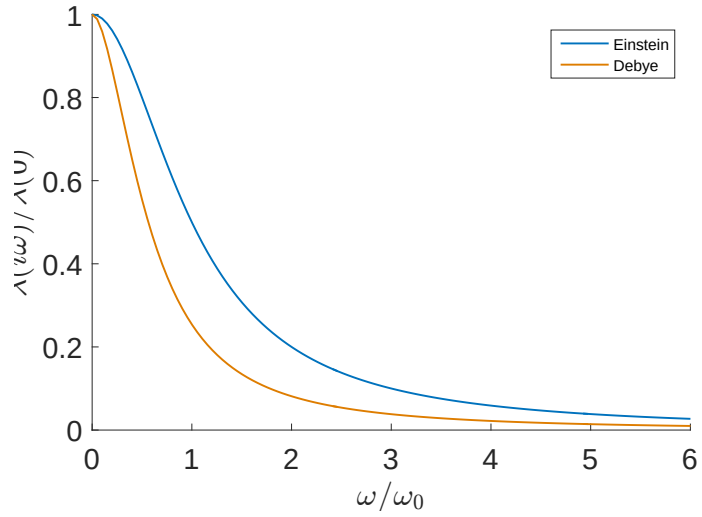

Figure 7. Strength of the electron-phonon interaction in the two phonon models. Parameters have been chosen so that the interactions match in the static limit and that the coefficients of ω^{-2} in the asymptotic expansion at $\omega \to \infty$ are the same. For the intermediate energies the interaction mediated by Einstein phonons is stronger.

where $+Ze$ is the ionic charge, ϵ_0 is the vacuum permittivity, k_s is the Thomas-Fermi screening length, M is the ionic mass, and N is the number of ions in the system. The takeaway from this equation is that for Debye phonons in the long wavelength limit $q \to 0$, the square of the electron-phonon coupling is linearly proportional to the momentum transfer,

$$g_{\mathbf{q}}^2 = aq = b\nu, \quad \text{for} \quad q \to 0, \tag{5.11}$$

with proportionality factors $a = (Ze^2/\epsilon_0 k_s^2)^2 N/2Mc$ and $b = a/c$. Using this, I obtain the interaction kernel for the Debye spectrum,

$$\lambda_D(\omega) = -\frac{bN(0)}{\pi^2 c^3}\int_0^{\omega_D} \frac{\nu^4}{\omega^2+\nu^2} = \lambda\left(1 - 3\left(\frac{\omega}{\omega_D}\right)^2\left\{1 - \frac{\omega}{\omega_D}\arctan\left(\frac{\omega_D}{\omega}\right)\right\}\right), \tag{5.12}$$

where $\lambda = bN(0)\omega_D^3/3\pi^2c^3$.

The interaction kernel for the Debye spectrum might at first sight look different from the Einstein kernel, but they actually have quite the same behaviour, as both are based on the phonon propagator, which is weighted with the Eliashberg function. Concentrating on imaginary frequencies $z{=}i\omega$, both kernels have a peak at $\omega{=}0$ and asymptotic behaviour $\lambda(i\omega) \sim 1/\omega^2$, when $\omega \to \infty$. Like the Einstein model, the Debye model has two independent parameters in the interaction kernel: λ determines the strength of the interaction in the static limit $\omega = 0$ and ω_D determines the scaling of the interaction as a function of frequency. Debye and Einstein interaction kernels with matching asymptotic behaviour and λ are compared in Fig. 7. The interaction kernel for the Einstein model has a simple analytical form, so below, if not stated otherwise, we use it to derive the results.

5.2 Eliashberg equations for a metal with finite bandwidth

If the interaction is taken to be of the form (5.6), which has no momentum dependence, the right-hand sides of the Eliashberg equations (4.26–4.28) do not depend on momentum. We can then drop the momentum indices from all the self-energy functions. The equation for χ, for example, reads

$$\chi_n = -T\sum_m \lambda(i\omega_n - i\omega_m)\int \mathrm{d}\xi\, \frac{\xi+\chi_m}{(Z_m\omega_m)^2+(\xi+\chi_m)^2+\phi_m^2}, \tag{5.13}$$

where n and m refer to Matsubara frequencies.

Before integrating over energy, the electron dispersion needs to be specified. Based on Bloch's theorem, electrons in a periodic lattice form bands, and these bands will have some width $D = \varepsilon_{\max} - \varepsilon_{\min}$. In metals the chemical potential μ is in the middle of the band. We can choose to measure our energies relative to the middle of the band, and then μ determines the deviation from that midpoint. We have already approximated the density of states as being constant. This is usually not a good approximation if we are taking into account the whole band, but it gives us some idea about the dependence of the different self-energy terms on the electronic structure.

With constant density of states, the self-consistency equation for χ is [31]

$$\begin{aligned}\chi_n &= -T\sum_m \lambda(i\omega_n - i\omega_m)\int_{-D/2}^{+D/2}\mathrm{d}\varepsilon\, \frac{\varepsilon-\mu+\chi_m}{(Z_m\omega_m)^2+(\varepsilon-\mu+\chi_m)^2+\phi_m^2}\\ &= -T\sum_m \lambda(i\omega_n - i\omega_m)A_1(m),\end{aligned} \tag{5.14}$$

where A_1 is

$$A_1(m) = \frac{1}{2}\log\left[\frac{(Z_m\omega_m)^2+\phi_m^2+(D/2-\mu+\chi_m)^2}{(Z_m\omega_m)^2+\phi_m^2+(D/2+\mu-\chi_m)^2}\right]. \tag{5.15}$$

The magnitude of A_1 depends on the inbalance in the density of states below and above the chemical potential. If μ=0, then χ_n=0 and $A_1(m) = 0$ is a solution for this equation. If $\mu \neq 0$, then χ tends to oppose μ and effectively decrease its magnitude. Because of the properties of the interaction kernel λ, $\chi_n \to 0$ as $|\omega_n| \gg \omega_D$.

Doing the same for ϕ and Z, we get [31]

$$\phi_n = \pi T\sum_m \lambda(i\omega_n - i\omega_m)\frac{\phi_m}{\sqrt{[Z_m\omega_m]^2+\phi_m^2}}A_0(m), \tag{5.16}$$

$$Z_n = 1 + \pi T\sum_m \lambda(i\omega_n - i\omega_m)\frac{\omega_m}{\omega_n}\frac{Z_m}{\sqrt{[Z_m\omega_m]^2+\phi_m^2}}A_0(m), \tag{5.17}$$

where

$$A_0(m) = \frac{1}{\pi}\left\{\arctan\left(\frac{D/2-\mu+\chi_m}{\sqrt{[Z_m\omega_m]^2+\phi_m^2}}\right)+\arctan\left(\frac{D/2+\mu-\chi_m}{\sqrt{[Z_m\omega_m]^2+\phi_m^2}}\right)\right\}. \tag{5.18}$$

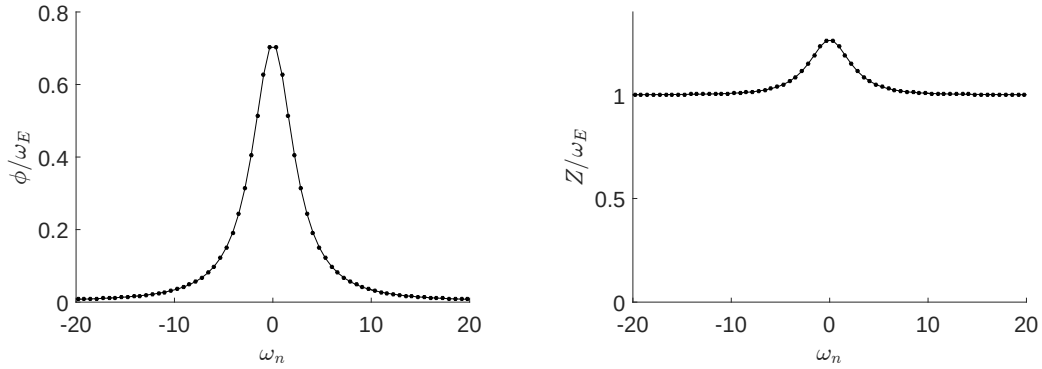

Figure 8. Shapes of $\phi(i\omega_n)$ (left) and $Z(i\omega_n)$ (right) for $\lambda = 0.4$ at $T = 0.1\omega_E$. For weak or intermediate -strength coupling the width of the peaks is independent of λ and cutoff can usually be chosen to be $10{-}20\omega_E$. Lines are drawn only to guide the eye, as the functions are defined at discrete points. The discretization is determined by the temperature.

In the infinite-bandwidth approximation $D \to \infty$, $A_0(m) = 1$ and $A_1(m) = 0$. In this approximation χ_m vanishes and there is also no shift in the chemical potential. We are then left with the two equations (5.16) and (5.17) in a simplified form. Even they can be condensed into one by defining $\Delta_n \equiv \phi_n/Z_n$. When $D \to \infty$, we have

$$Z_n\Delta_n = \pi T \sum_m \lambda(i\omega_n - i\omega_m)\frac{\Delta_m}{\sqrt{\omega_m^2 + \Delta_m^2}}. \tag{5.19}$$

Substituting the equation for Z in this, we are left with the equation [32]

$$\Delta_n = \pi T \sum_m \lambda(i\omega_n - i\omega_m)\frac{\Delta_m - \dfrac{\omega_m}{\omega_n}\Delta_n}{\sqrt{\omega_m^2 + \Delta_m^2}}, \tag{5.20}$$

which now only depends on Δ, and not on any other function. Example solutions of ϕ and Z are shown in Fig. 8. If we removed the $-\omega_m\Delta_m/\omega_n$ -term, which comes from the Z-function, we would obtain a BCS-like self-consistency equation.

5.3 Transition temperature

Near the transition temperature T_c, we can neglect the Δ_m in Eq. (5.20) in the denominator. The self-consistency equation (5.20) at the transition temperature can be written explicitly as

$$\Delta_n = \sum_{m=-\infty}^{\infty} \frac{\lambda\omega_E^2}{\omega_E^2 + 4\pi^2 T_c^2 (m-n)^2} \left(\frac{\Delta_m}{|2m+1|} - \frac{2m+1}{|2m+1|} \frac{\Delta_n}{2n+1} \right) \tag{5.21}$$

In this equation we have two dimensionless parameters, λ and T_c/ω_E, which are usually not independent of each other, as they depend on the same material parameters.

5.3.1 Strong coupling

To study the difference between Eliashberg theory and BCS theory, we first choose the limit in which $T_c/\omega_E \gg 1$, which can be realized by either keeping λ fixed and taking $\omega_E \to 0$ or keeping ω_E fixed and taking $g \to \infty$. By noting that $m{=}n$ term in the sum (5.21) is zero, and restricting the sum to $m{\neq}n$, we can neglect the constant term in the interaction kernel[32]:

$$\Delta_n = \frac{\lambda\omega_E^2}{4\pi^2 T_c^2} \sum_{m\neq n} \frac{1}{(m-n)^2} \left(\frac{\Delta_m}{|2m+1|} - \frac{2m+1}{|2m+1|} \frac{\Delta_n}{2n+1} \right) \tag{5.22}$$

The above equation can be written as an eigenvalue equation with eigenvalues $\alpha = \lambda/4\pi^2 T_c^2$. Value of α does not depend on any material parameters, so it is possible to first solve α numerically, and then T_c from α.

In the numerics we must choose some cutoff N for the summation. Then the equation will have $2N$ eigenvalues and we are faced with the question: which one of them corresponds to the physically relevant T_c? Near the transition temperature Z_n can be solved independently of ϕ_n and can be regarded as a fixed function in the ϕ-equation (5.16). Taking the strong-coupling limit of that equation, one can then use the Perron-Frobenius theorem, which states that for strictly positive matrices the eigenvector corresponding to the largest eigenvalue is real and positive[33]. The other eigenvectors are oscillatory. It is then natural to choose the largest eigenvalue as the one corresponding to the critical temperature.

The critical temperature can then be calculated from (5.22) by the power iteration algorithm, which means that we solve Δ by iteration

$$\Delta^{i+1} = \frac{f(\Delta^i)}{\|f(\Delta^i)\|}, \tag{5.23}$$

where $f(\Delta^i)$ corresponds to the rhs of (5.22) without the unknown constant in front of the summation, and with Δ replaced with the ith iteration Δ^i. Here Δ is understood as a vector with the components Δ_n. In (5.23) Δ^i is also normalized at every iteration. Δ

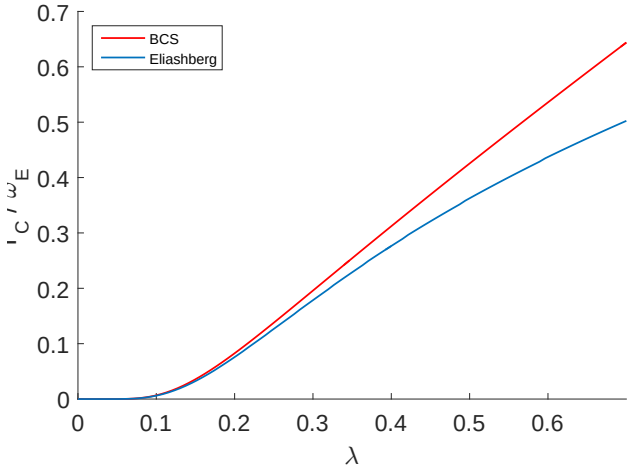

Figure 9. Critical temperature in BCS and Eliashberg models. In the weak effective interaction regime, superconductivity is exponentially suppressed in both models. In the strong coupling regime, the results diverge, with Eliashberg theory predicting smaller T_C.

is then obtained as the limit of this sequence and T_c can be calculated from

$$\frac{\lambda\omega_E^2}{4\pi^2 T_c^2} = \frac{\Delta_n}{f(\Delta)_n}, \quad \text{for any } n. \tag{5.24}$$

The result for the critical temperature in this limit is[32]

$$T_c \approx 0.258\omega_{\mathrm{E}}\sqrt{\lambda}. \tag{5.25}$$

This result should be contrasted with the BCS strong coupling limit $T_c = \lambda\omega_D$, which is linear in λ.

5.3.2 Weak coupling

When the interaction kernel cannot be simplified as in (5.22), the problem of finding the critical temperature does not quite turn into an eigenvalue problem as the interaction kernel depends on T_c in a non-linear way. The equation is still linear in Δ, and the power iteration algorithm can be modified to find an approximate solution for T_c. T_c can be solved iteratively by starting from some initial guess T_0 and approximating the interaction kernel at every iteration by

$$\frac{\lambda\omega_E^2}{\omega_E^2 + 4\pi^2 T_c^2 (m-n)^2} \approx \frac{\lambda\omega_E^2}{4\pi^2 T_{k+1}^2} \frac{1}{(\omega_E/4\pi^2 T_k)^2 + (m-n)^2}, \tag{5.26}$$

so that we can take T_{k+1} out of the sum. T_{k+1} can then be solved as in (5.24), but now the solution depends on an earlier value T_k. This approximation is bad if T_k is far from T_c, but gets exact as the iteration in k converges. In practice the iteration seems to converge

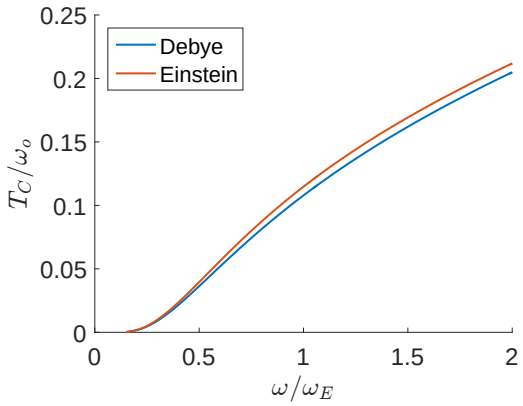

Figure 10. Transition temperature in the Einstein and Debye phonon models. In the y-axis scale, ω_0 stands for ω_E or ω_D, depending on the model. The curve is very similar for both model dispersions.

well regardless of the initial guess.

The results for T_c with fixed ω_E are shown in Fig. 9. For large λ, the square root behaviour is clearly seen and for the weak coupling, the behaviour is exponentially suppressed, as in the BCS case. If we choose the BCS interaction parameter as the λ used here, then the BCS and Eliashberg results coincide in the weak coupling limit. The exponential behaviour is difficult to calculate numerically, because the number of relevant Matsubara points is inversely proportional to the critical temperature. To put it the other way, the number of points increases exponentially as λ decreases.

When the interaction is strong, the Eliashberg theory predicts a smaller T_C than the BCS theory. In small part this is because of the renormalization function Z which increases the denominator in the Eliashberg equations, effectively decreasing the interaction constant as in Eq. (4.37). The more important factor is the frequency dependence of the interaction kernel $\lambda(z)$ and ϕ, both of which are approximated constant (except for the cutoff) in frequency in the BCS model.

Let us then compare the Debye and the Einstein models. By again fixing the asymptotic and static limits to be same in both models, we can compare them. There is not much of a difference in the transition temperature between the two models as shown in the Fig. 10.

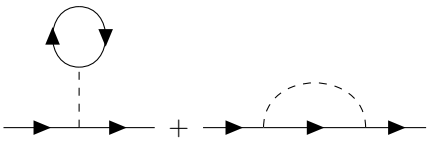

Figure 11. Hartree and Fock self-energy from Coulomb interaction. In the jellium model, the Hartree term on the left is cancelled by the contribution from the positive background charge.

5.4 Coulomb interaction

Superconductivity is caused by an attractive interaction. In a lattice the electrons also interact via Coulomb interaction, which is repulsive. Intuitively it is clear that this repulsion weakens the superconducting state and lowers the transition temperature. We would like to know the exact effect of this repulsion, so let us consider the Coulomb interaction in more detail.

If we think of the possible Feynman diagrams, then the contributions to the irreducible electron self-energy from Coulomb interaction can be collected into the two categories shown in Fig. 11, the Hartree and Fock terms. The propagators and vertices shown in the figure are bare, but the general diagrams can be obtained from these two by dressing them in a suitable way.

If we would try to calculate the Hartree term, we would notice that it is divergent. This is because we are only considering neutral phonons and negatively charged electrons explicitly, even though the complete system is neutral. To remove the divergence, we must add a positive background charge. The jellium model assumes that the background charge is spread out uniformly and because the ions are heavy, the background stays fixed. In the jellium model it can then be shown that the Hartree term and the term from the ionic background cancel exactly.[34]

Without the Hartree term, the only contribution to the self-energy comes from the self-consistent Fock diagram as in the phonon case. Writing the total self-energy as a sum $\Sigma = \Sigma^{ph} + \Sigma^c$ and also by dividing each Nambu space component, we get

$$\phi^c(\mathbf{p}) = -\int \frac{\mathrm{d}^3\mathbf{p}'}{(2\pi)^3} T\sum_m V^c(\mathbf{p}-\mathbf{p}')\frac{\phi(\mathbf{p}',i\omega_m)}{\Omega(\mathbf{p}',i\omega_m)}, \tag{5.27}$$

$$[1-Z(\mathbf{p})]^c\omega_n = \int \frac{\mathrm{d}^3\mathbf{p}'}{(2\pi)^3} T\sum_m V^c(\mathbf{p}-\mathbf{p}')\frac{Z(\mathbf{p}',i\omega_m)\omega_m}{\Omega(\mathbf{p}',i\omega_m)}, \tag{5.28}$$

$$\chi(\mathbf{p})^c = +\int \frac{\mathrm{d}^3\mathbf{p}'}{(2\pi)^3} T\sum_m V^c(\mathbf{p}-\mathbf{p}')\frac{\xi_{\mathbf{p}'}+\chi(\mathbf{p}',i\omega_m)}{\Omega(\mathbf{p}',i\omega_m)}, \tag{5.29}$$

where, on the right hand side, we have the total self-energy components, which include both Coulomb and electron-phonon contributions. On the left hand side we only have the Coulomb parts. Because we consider the Coulomb interaction instantanious i.e., assume $c \gg v_F$, where c is the speed of light, there is no frequency dependence in the Coulomb interaction. The summand in (5.28) is then odd in Matsubara frequencies and the sum

vanishes. For this reason there is no Coulomb contribution to Z.

Coulomb contribution to χ does not vanish, and can be quite large. The difference between the normal state χ_N^c and the superconducting state χ_{SC}^c on the other hand, is small (in metals of order Δ/ε_F[28]), and the explicit mention of χ can be removed by including it in the dispersion by redefining $\xi_{\mathbf{p}}+\chi(\mathbf{p}) \to \xi_{\mathbf{p}}$. The effect of $\chi_{SC}^c-\chi_N^c$ would be to change the effective electron mass and shift the chemical potential[34], the magnitude of the shift being in metals of the order of Δ^2/ε_F. The main effects in superconductivity are created by the electron-phonon interaction and we are considering Coulomb interaction only as an modifier to those effects. The normal contributions to the Coulomb self-energy are then removed and the only significant part is the anomalous part ϕ_c.

5.5 Anderson-Morel pseudopotential

Examining the two components of ϕ corresponding to the Coulomb and the electron-phonon interactions, we notice that the electron-phonon part has a frequency dependence but no momentum dependence, and for the Coulomb part the reverse is true:

$$\phi(\mathbf{p}, i\omega_n) = \phi_n^{\mathrm{ph}} + \phi^{\mathrm{c}}(\mathbf{p}). \tag{5.30}$$

The lack of frequency dependence in the Coulomb kernel causes practical problems because the energy scale that should be considered in the numerics gets large. For phonon interaction the summation can be typically cut off at $10\,\omega_D$ because of the frequency dependent kernel, but for Coulomb interaction, energies of the order of the electronic bandwidth $\omega \sim \varepsilon_F$ should be taken into account. To solve this problem, the method of Morel and Anderson[11] can be used. In this method, the Coulomb interaction with infinite range in frequency space is replaced by a pseudopotential with a small cutoff. The presentation given here follows the article by Schrieffer et al.[28], but I reformulate it in Matsubara frequencies.

When compressing the Coulomb interaction into a pseudopotential, the strength of the interaction is also reduced. So, while pseudopotential is basically a calculational trick, it also reveals that the larger the electronic energies are in comparison to the phonon energies, the weaker the effect Coulomb interaction has on the order parameter Δ. This is at least part of the reason why Coulomb interaction is relatively insignificant with respect to superconductivity.

The summation over frequencies includes both positive and negative frequencies, but it can be folded over and expressed as a summation over the positive frequencies. All the self-energy functions are even in ω_m, so only the interaction kernel is affected. We can also add a cutoff N, chosen so that ϕ_n^{ph} is effectively zero for $|\omega_n| > \omega_N$. As stated above, $\omega_N = 10\,\omega_D$ is typically enough. After these manipulations, we have for the electron–phonon part

$$\phi_n^{\mathrm{ph}} = -T \sum_{m=1}^{N} \int \frac{\mathrm{d}^3\mathbf{p}'}{(2\pi)^3} \left[\lambda(n-m) + \lambda(n+m)\right] \frac{\phi_m(\mathbf{p}')}{[Z_m\omega_m]^2 + \xi_{p'}^2 + \phi_m^2(\mathbf{p}')}. \tag{5.31}$$

For ϕ^{c} the self-consistency equation can be divided into two parts at the cutoff N. Above the cutoff, $Z \approx 1$ and $\phi_n^{\mathrm{ph}} \approx 0$ and the only self-energy part which survives is ϕ^{c}. The frequencies are large above the cutoff, so ϕ can also be neglected in the denominator above the cutoff. The self-consistency equation is

$$\phi^{\mathrm{c}}(\mathbf{p}) = -2T \int \frac{\mathrm{d}^3\mathbf{p}'}{(2\pi)^3} V^c(\mathbf{p}-\mathbf{p}') \left\{ \sum_{m=1}^{N} \frac{\phi_m(\mathbf{p}')}{[Z_m\omega_m]^2 + \xi_{\mathbf{p}'}^2 + \phi_m^2(p')} + \sum_{m=N+1}^{\infty} \frac{\phi^{\mathrm{c}}(\mathbf{p}')}{\omega_m^2 + \xi_{\mathbf{p}'}^2} \right\}, \quad (5.32)$$

In the isotropic case, the interaction can be averaged over the angles,

$$\phi^{\mathrm{c}}(p) = 2T \int_0^{\infty} \frac{\mathrm{d}p'}{2\pi^2} V(p,p') \left\{ \sum_{m=1}^{N} \frac{\phi_m(p')}{[Z_m\omega_m]^2 + \xi_{p'}^2 + \phi_m^2} + \sum_{m=N+1}^{\infty} \frac{\phi^{\mathrm{c}}(p')}{\omega_m^2 + \xi_{p'}^2} \right\}. \quad (5.33)$$

We describe the screened Coulomb interaction between the electrons by a Thomas-Fermi potential[35]

$$V^{\mathrm{c}}(\mathbf{q}) = \frac{e^2}{\epsilon_0(q^2 + k_s^2)}, \quad (5.34)$$

where e is the elementary charge, ϵ_0 is the vacuum permittivity and k_s is the Thomas-Fermi wavevector. The screening length is inversely proportional to k_s. With this potential, the angle-averaged Coulomb interaction is

$$V(p,p') \equiv \int \frac{\mathrm{d}\Omega}{4\pi} V^{\mathrm{c}}(\mathbf{p}-\mathbf{p}') = \frac{e^2}{4\epsilon_0 pp'} \ln\left(\frac{(p-p')^2 + k_s^2}{(p+p')^2 + k_s^2} \right). \quad (5.35)$$

Eq. (5.33) can be formally written as a matrix equation,[28]

$$\phi^{\mathrm{c}} = VF - \Omega\phi^{\mathrm{c}}, \quad (5.36)$$

with p and p' viewed as matrix indices and the summation over the index represented by the integral. Here, F is a vector containing the contribution to ϕ_c below the cutoff

$$F(p) = 2T \sum_{m=1}^{N} \frac{\phi_m(p)}{[Z_m\omega_m]^2 + \xi_p^2 + \phi_m^2(p)}, \quad (5.37)$$

and Ω is a matrix containing the contribution above the cutoff, multiplied with the Coulomb interaction matrix V,

$$\Omega(p,p') = 2V(p,p')\, T \sum_{m=N+1}^{\infty} \frac{1}{\omega_m^2 + \xi_{p'}^2}. \quad (5.38)$$

In this context, ϕ_c is a vector and it can be solved from Eq. (5.36) as

$$\phi^{\mathrm{c}} = (1+\Omega)^{-1} VF \equiv U^* F, \quad (5.39)$$

where the matrix inverse in $U^* = (1+\Omega)^{-1}V$ exists because the Coulomb interaction is

repulsive, and therefore $\Omega(p,p') \geq 0$ for all p and p'. U^* is the Anderson-Morel pseudopotential, and it can be calculated from the integral equation

$$U^*(p,p') = V(p,p') - 2T\int_0^\infty \frac{\mathrm{d}p''}{2\pi^2} \sum_{m=N+1}^{\infty} V(p,p'') \frac{U^*(p'',p')}{\omega_m^2 + \xi_{p''}^2}, \tag{5.40}$$

from which we can see that the Coulomb interactions above the cutoff are taken into account by reducing the effective potential U^* below the cutoff. After U^* has been solved, the equation for ϕ_c becomes

$$\phi^{\mathrm{c}}(p) = -\int_0^\infty \frac{\mathrm{d}p'}{2\pi^2} U^*(p,p')\, T \sum_{|\omega_m|<\omega_N} \frac{\phi_m(p')}{[Z_m\omega_m]^2 + \xi_{p'}^2 + \phi_m^2}, \tag{5.41}$$

which can be included in the Eliashberg equations.

5.6 Pseudopotential in metals

Above, the treatment of the Coulomb interaction is quite general, as we have not even specified the dispersion relation. In metals, the Thomas-Fermi wavevector k_s is of the same order of magnitude as the Fermi momentum p_F. In Eq. (5.40) most of the contribution comes from the region near the Fermi surface and we can thus approximate $U^*(p,p') \approx U^*(p,p_F)$ and similarly for V. If we are also only interested in $\phi_c(p)$ near the Fermi surface, we can also set $p = p_{FB}$ in $U^*(p,p_F)$. Thus, in this approximation, the angle-averaged potentials V and U^* are constant in the regions of interest,

$$\mu \equiv V(p_F,p_F) \quad \text{and} \quad \mu^* \equiv U^*(p_F,p_F). \tag{5.42}$$

μ^* can be now solved from Eq. (5.40),

$$\mu^* = \frac{\mu}{1 + 2\mu\int \frac{\mathrm{d}p'}{2\pi^2} T \sum_{m=N+1}^{\infty} \frac{1}{\omega_m^2 + \xi_{p'}^2}}. \tag{5.43}$$

Here μ should not be confused with the chemical potential. It is the magnitude of the angle-averaged Coulomb interaction and μ^* is the strength of the corresponding pseudopotential. The Coulomb contribution to ϕ is

$$\phi^{\mathrm{c}} = -\mu^* \int \frac{\mathrm{d}^3\mathbf{p}'}{(2\pi)^3} T \sum_{m=1}^{N} \frac{\phi_m}{[Z_m\omega_m]^2 + \xi_{p'}^2 + \phi_m^2}, \tag{5.44}$$

and the Eliashberg equation for the total ϕ is

$$\phi(i\omega_n) = T\sum_m \left[\lambda(i\omega_n - i\omega_m) - N(0)\mu^*\right] \frac{\phi_m}{\sqrt{(Z_m\omega_m)^2 + \phi_m^2}}. \tag{5.45}$$

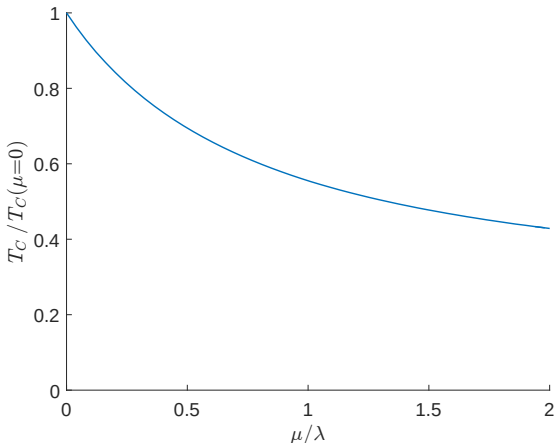

Figure 12. Effect of Coulomb interaction on T_C.

Within this approximation, the interaction is only modified by an addition of a constant, but only for ϕ, as the Coulomb potential is not added to the self-consistency equations for the other self-energy components.

For a Fermi-surface with finite bandwidth D and constant density of states, we can also do the momentum integration of (5.43). We get [31]

$$\mu^* = \frac{\mu}{1 + 2\mu N(0)\pi T \sum_{m=N+1}^{\infty} \frac{1}{\omega_m} \arctan\left(\frac{D}{2\omega_n}\right)}. \tag{5.46}$$

The arctangent-function serves as a soft cutoff, and is needed for the Matsubara summation to converge. For infinite bandwidth, an artificial cutoff would have to be introduced. The above Matsubara summation is a little more involved, but the asymptotical result is

$$\mu^* = \frac{\mu}{1 + \mu N(0) \log(D/2\omega_c)}. \tag{5.47}$$

The bandwidth is of the order of Fermi energy and the cutoff of the order of Debye energy. From this expression we can see that the larger the discrepancy between the two scales, the more the pseudopotential is reduced and with it, the Coulomb effects.

Numerical results from the linearized equations for the transition temperature are shown in Fig. 12. For small U the reduction is linear. Superconductivity does not seem to disappear even when $U > \lambda$, but at large U the algorithm based on fixed-point iteration starts to oscillate, and a damping factor has to be used to converge the solution. The iteration is then modified to the form

$$\Delta_{i+1} = (1 - \epsilon) f(\Delta_i) + \epsilon \Delta_i, \tag{5.48}$$

where $\epsilon \in [0, 1]$ is the damping. $\epsilon = 0$ is the original iteration algorithm. At $U \approx 2$, the damping as strong as $\epsilon = 0.99$ had to be used. Based on the instability in the numerics, it is possible that the superconducting phase is physically unstable in such a case.

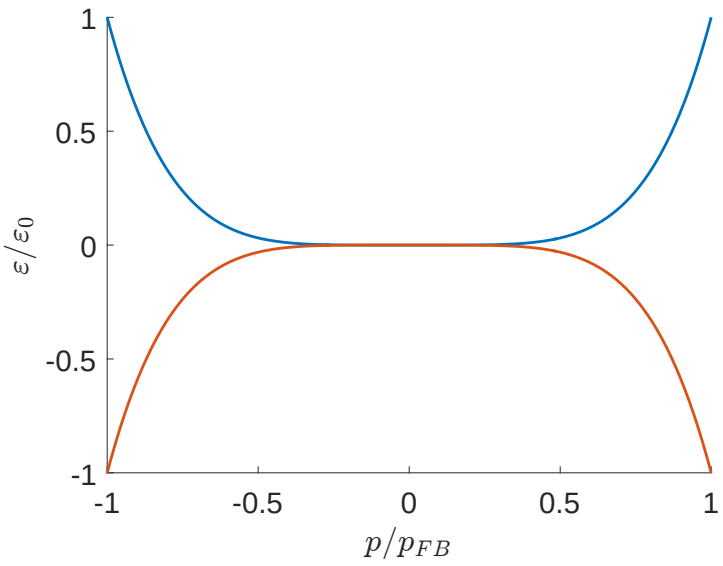

Figure 13. Flat band with the dispersion $\varepsilon(p) = \pm\varepsilon_0(p/p_{FB})^5$. The chemical potential is at $\varepsilon = 0$.

6 Superconductivity in ideal flat band

So far, I have only considered superconductivity in metals, in which the electronic bandwidth is large compared to the Debye energy. This is natural, in the sense that the most conventional superconductors are metals and the BCS and Eliashberg theories were originally developed to explain the superconductivity in metals.

There is, however, no real reason why the Eliashberg theory would not apply to other kinds of systems also, provided the approximations of the theory are critically evaluated. Based on the BCS expression for the effective interaction strength which is proportional to the density of electron states, one possible criterion for the choice of the system is a high density of states.

Density of states is inversely proportional to the derivative of the dispersion relation, $N(0) \sim [\mathrm{d}\varepsilon(p)/\mathrm{d}p]^{-1}$, so the density of states is high when the energy varies as little as possible near the chemical potential. A prototypical dispersion to achieve this is

$$\varepsilon(\mathbf{p}) = \varepsilon_0 \left(\frac{p}{p_{FB}}\right)^N, \tag{6.1}$$

where N is some large integer, and ε_0 and p_{FB} are the energy and momentum scales,

respectively, of the system. When $p < p_{FB}$, the dispersion is very flat, so that $\varepsilon(\mathbf{p}) \ll \varepsilon_0$. $N = 5$ is already large enough to achieve quite a flat dispersion when $p < 0.5\, p_{FB}$ (Fig. 13). We also include a second band with an inverse dispersion $\varepsilon(\mathbf{p}) = -\varepsilon_0 \left(\frac{p}{p_{FB}}\right)^N$ as shown in the figure. The existence of this second band creates a symmetry between the unoccupied and occupied states, which removes the need for equations of χ and μ.

This kind of flat band dispersion is obtained in many places, most notably in graphite at interfaces, surfaces and lateral edges and also in periodically strained graphene[12, 36]. In these cases the momentum is restricted to two dimensions, and in the following, I only consider 2D momentum.

In the limit $N \to \infty$, the dispersion becomes a completely flat infinite well:

$$\varepsilon(\mathbf{p}) = \begin{cases} 0 & |\mathbf{p}| < p_{FB} \\ \infty & |\mathbf{p}| > p_{FB} \end{cases}. \tag{6.2}$$

As this is the simplest case, I first consider the effect of different factors to superconductivity with this model dispersion. In Sec. 6.4 I consider finitely flat dispersions.

The BCS self-consistency equation for flat band is achieved by replacing the usual dispersion in (2.28) with the dispersion (6.2) and by limiting the momentum to two dimensions. At zero temperature, we get [12]

$$\Delta_0 = \int_{|\mathbf{p}|<p_{FB}} \frac{\mathrm{d}^2\mathbf{p}}{(2\pi)^2} \frac{V}{2} = \frac{V p_{FB}^2}{8\pi}, \tag{6.3}$$

where V is the strength of the interaction. In contrast to exponentially suppressed Δ in metals, in a flat band the strength of superconductivity grows linearly with respect to the flat band area πp_{FB}^2 and interaction strength V. Also, this expression does not depend on phonon energies, except for the possible dependence hidden in V. The transition temperature is $T_C = 2\Delta_0$.

6.1 Eliashberg theory

We can also do Eliashberg theory simply by inserting the dispersion (6.2) into the Eliashberg equations (4.26–4.28) and again limiting the momentum integration to 2D. This is a very simple way of projecting the high-energy states out from the Green's functions and the validity of this projection should be checked in any real system.

The existence of two bands can be included in the Eliashberg equations by adding a summation over bands to the momentum integration. With the two bands symmetric around the chemical potential, the self-consistency equations for χ and μ vanish because there is no imbalance between the occupied and unoccupied states. The other two Eliash-

berg equations obtain an extra factor of 2 from the summation over bands, and are

$$\phi_n = \frac{p_{FB}^2}{2\pi} T \sum_m g^2 D_E(i\omega_m - i\omega_n) \frac{\phi_m}{[Z_m\omega_m]^2 + \phi_m^2} \tag{6.4}$$

$$Z_n = 1 + \frac{p_{FB}^2}{2\pi} \frac{T}{\omega_n} \sum_m g^2 D_E(i\omega_m - i\omega_n) \frac{Z_m\omega_m}{[Z_m\omega_m]^2 + \phi_m^2}, \tag{6.5}$$

where Einstein spectrum was chosen for analytical convenience. Writing the equation for ϕ in terms of the interaction kernel

$$\lambda(i\omega_m - i\omega_n) = \frac{\lambda\omega_E^2}{\omega_E^2 + (\omega_m - \omega_n)^2}, \tag{6.6}$$

we find the dimensionless interaction constant

$$\lambda = \frac{g^2 p_{FB}^2}{\pi\omega_E^2}, \tag{6.7}$$

and the equation itself becomes

$$\phi_n = T \sum_m \lambda(i\omega_m - i\omega_n) \frac{\phi_m \omega_E}{[Z_m\omega_m]^2 + \phi_m^2}. \tag{6.8}$$

Although the loose ω_E in the numerator might seem weird, in this way a dimensionless interaction constant is obtained. That this is the natural choice can be seen by writing the linearized equations at the transition temperature and pairing each ω_E with T_C,

$$\phi_n = \lambda \frac{\omega_E}{T_c} \sum_m \left[1 + 4\pi^2 (m-n)^2 \left(\frac{T_c}{\omega_E} \right)^2 \right]^{-1} \frac{\phi_n}{Z_m^2 (2m+1)^2}, \tag{6.9}$$

$$Z_n = 1 + \lambda \frac{\omega_E}{T_c} \frac{1}{(2n+1)\pi^2} \sum_m \left[1 + 4\pi^2 (m-n)^2 \left(\frac{T_c}{\omega_E} \right)^2 \right]^{-1} \frac{1}{Z_m (2m+1)}, \tag{6.10}$$

from which we can read the relevant dimensionless parameters as being T_C/ω_E and λ as defined above.

In this case, Z_n cannot be removed from the equations as easily as in (5.20), so the asymptotic behaviour is harder to calculate. From numerical calculations, it is seen that the results coincide in the weak coupling limit with the BCS results (Fig. 14a). In the strong-coupling limit the transition temperature grows very slowly as compared to the Fermi-surface result. At Fermi-surface $T_C \sim \lambda^{1/2}$ and for the flat band $T_C \sim \lambda^{0.2}$ based on numerical calculations. The temperature dependence of the gap Δ_0 has the usual form as shown in the Fig. 14b.

The BCS limit can also be obtained analytically by taking the static limit, $\lambda(z) \approx \lambda$, in which ϕ and Z also have no frequency dependence. When $\lambda \ll 1$, $Z \approx 1$ and the equation for ϕ is

$$\phi = T \sum_m \lambda \frac{\phi\, \omega_E}{\omega_m^2 + \phi^2} = \frac{\omega_E \lambda}{2\phi} \tanh\left(\frac{\phi}{2T} \right). \tag{6.11}$$

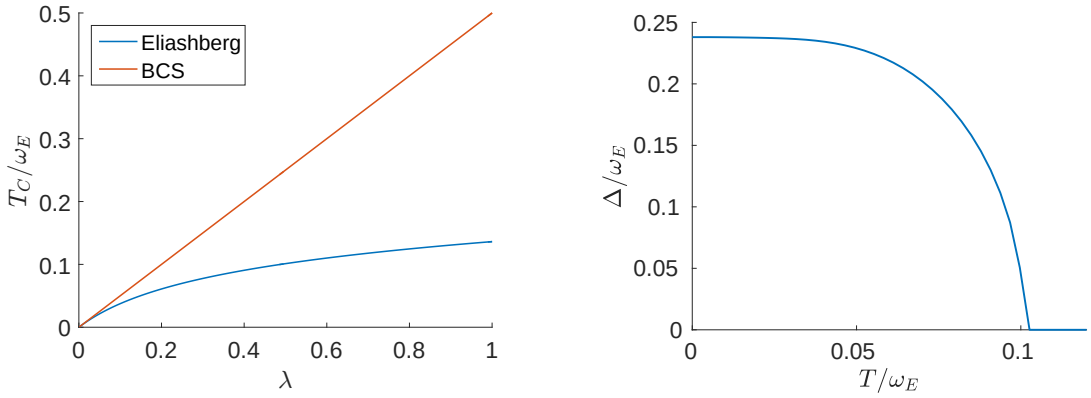

(a) **(b)**

Figure 14. Left: Transition temperature in with fixed ω_E and variable λ. The solution coincides with BCS result at weak coupling $\lambda \to 0$. Right: Temperature dependence of the superconducting gap in flat band with $\lambda = 0.5$.

At zero temperature, the superconducting gap is

$$\Delta_0 \approx \phi_0 = \int_{-\infty}^{\infty} \frac{\mathrm{d}\omega}{2\pi} \frac{\lambda\phi\omega_E}{\omega^2 + \phi^2} = \frac{\lambda}{2}\omega_E. \tag{6.12}$$

The transition temperature is obtained by expanding the inverse hyperbolic tangent at $\phi = 0$.

$$T_C = \frac{\lambda}{4}\omega_E \quad \text{or} \quad 2T_C = \Delta_0, \tag{6.13}$$

as obtained from the BCS theory [Eq. (6.3)] with interaction strength $V = g^2/2\omega_E$.

6.2 Debye phonon model

In the Debye phonon model, the phonons have a maximum momentum q_M, which is detemined by the condition $cq_M = \omega_D$. In a flat band, the maximum phonon momentum is not restricted by the requirement $cq \leq \omega_D$, but by the flat band diameter $2p_{FB}$. The order of magnitude of the Debye phonon energy in a flat band is

$$\omega_0 \equiv cp_{FB} = \omega_D \frac{p_{FB}}{q_M} \ll \omega_D, \tag{6.14}$$

if $q_M \gg p_{FB}$.

What is the effect of this restriction on the interaction strength? We can estimate it by neglecting the momentum dependence in the self-energy, so that the interaction can be averaged over the flat band. Assuming that $g_{\mathbf{q}}^2 = aq$ and $\omega_q = cq$, the average is

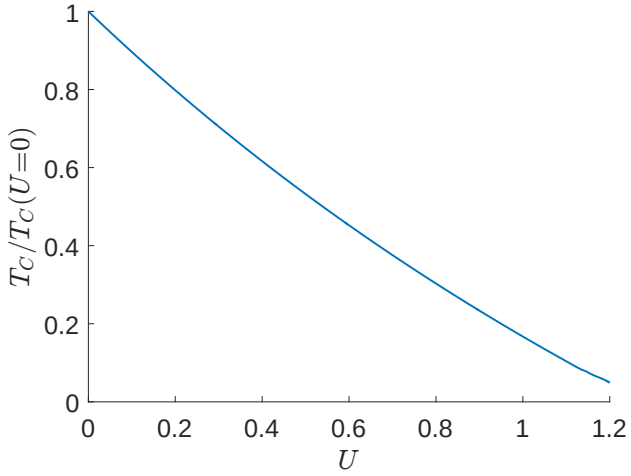

Figure 15. Effect of the Coulomb interaction on T_C in a flat band for $\lambda = 1$. T_C decreases almost linearly in U. Approximation (6.19) was not used, but the Matsubara sum was calculated numerically.

calculated as

$$\begin{aligned}
&\frac{1}{\pi p_{FB}^2}\int_{p<p_{FB}} \mathrm{d}^2\mathbf{p} \int_{p'<p_{FB}} \frac{\mathrm{d}^2\mathbf{p}'}{(2\pi)^2}\, g^2_{\mathbf{p}-\mathbf{p}'} D(\mathbf{p}-\mathbf{p}', i\nu_n) \\
=&\frac{a}{2\pi^2 p_{FB}^2 c}\int_0^{p_{PF}} \mathrm{d}p \int_0^{p_{PF}} \mathrm{d}p' \int_{|p-p'|}^{p+p'} \mathrm{d}q\, \frac{q^3}{q^2+(\nu/c)^2} \\
=&\frac{a p_{FB}^3}{2\pi^2 c}\int_0^1 \mathrm{d}x \int_0^1 \mathrm{d}y \int_{|x-y|}^{x+y} \mathrm{d}u\, \frac{u^3}{u^2+(\nu/c p_{FB})^2}.
\end{aligned} \tag{6.15}$$

Here it can already be seen that the relevant scale for energy ν is ω_0 as defined in (6.14). By taking the zero frequency limit $\nu = 0$ of the above expression we get the dimensionless interaction parameter

$$\lambda = \frac{a p_{FB}^3}{2\pi^2 c \omega_0^2}, \tag{6.16}$$

where the factor of 2 coming from the summation over the bands is included.

With a small flat band momentum as compared to q_M, ω_0 is small compared to ω_D. Then at low energies the effective interaction is stronger than what would be obtained if we had ω_D instead of ω_0. The tradeoff is that it dies off faster at large frequencies. These two behaviours oppose each other.

6.3 Coulomb pseudopotential in flat band

It is also possible to take the Coulomb interaction into account in the flat band, using the pseudopotential as in a metal. Again we use the Thomas-Fermi potential of Eq. (5.34) as a model for the Coulomb interaction. We assume that the screening length is very small, $k_s \gg p_{FB}$, so that the interaction is effectively constant on the flat band. The strength

of the interaction is

$$U \approx U(0,0) = \frac{e^2}{\epsilon_0 k_s^2}. \tag{6.17}$$

For a flat band, Eq. (5.43) gives

$$U^* = \frac{U}{1 + \frac{p_{FB}^2}{2\pi} UT \sum_{m=N+1}^{\infty} \frac{1}{\omega_m^2}}. \tag{6.18}$$

The summation can be expanded asymptotically in the cutoff N:

$$\sum_{m=N+1}^{\infty} \frac{1}{(2m+1)^2} = \frac{1}{4N} + \mathcal{O}(\frac{1}{N^3}), \tag{6.19}$$

so instead of a logaritmic dependence on ε_F/ω_c as in metals, we have a linear dependence on p_{FB}^2/ω_c in the denominator:

$$U^* = \frac{U}{1 + \frac{U p_{FB}^2}{4\pi^2 \omega_c}}. \tag{6.20}$$

In comparison to the Fermi surface case (5.47) the denominator of (6.20) depends linearly on the ratio of electron and phonon energies, and not logaritmically as for the Fermi surface. This means that for flat bands with a large area, the reduction of Coulomb effects is strong.

Numerical results for the effect on T_c are shown in Fig. 15. The effect seems to be similar to the Fermi surface case: superconductivity is suppressed by the Coulomb interaction, but because of the pseudopotential effect, the interaction effects are reduced somewhat and we can have superconductivity when $U/\lambda > 1$. It is not clear what happens after $U \geq 1.2$ as the numerics become difficult to do with low T_C and with ϕ^c and ϕ_0^{ph} having similar magnitudes.

6.4 Finite N

Let us examine the Eliashberg equations for an approximate flat band with 2D dispersion $\varepsilon(\mathbf{p}) = \varepsilon_0 (p/p_{FB})^N$, where ε_0 defines the energy scale of the flat band and $N \geq 2$ is an integer. It is possible to integrate out the momentum dependence by using the integral identity

$$\int_0^\infty \mathrm{d}x \, \frac{x}{x^{2N} + A} = \frac{1}{2} \frac{\pi}{N \sin(\pi/N)} \frac{1}{A^{1-1/N}}, \tag{6.21}$$

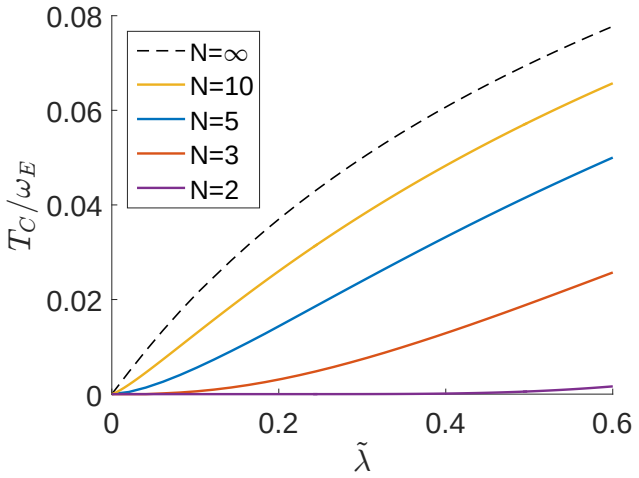

Figure 16. Critical temperature for a finitely flat band with dispersion $(p/p_{FB})^N$ with $\chi_m = 0$. The coupling constant is $\tilde{\lambda}$ as defined below Eq. (6.24). For $N = 2$ superconductivity is exponentially suppressed within the shown range of $\tilde{\lambda}$.

For ϕ_n we can write

$$\begin{aligned}\phi_n &= T\sum_m \frac{2g^2\omega_E}{\omega_E^2+(\omega_m-\omega_n)^2}\int\frac{\mathrm{d}^2\mathbf{p}}{(2\pi)^2}\frac{\phi_m}{(Z_m\omega_m)^2+\varepsilon_0^2\left(\frac{p}{p_{FB}}\right)^2+\phi_m^2}\\ &= \frac{g^2p_{FB}^2}{2\pi\omega_E}T\sum_m\left[1+\left(\frac{\omega_m-\omega_n}{\omega_E}\right)^2\right]^{-1}\frac{2\phi_m}{\varepsilon_0^2}\int_0^\infty \mathrm{d}x\,\frac{x}{x^{2N}+(Z_m\omega_m/\varepsilon_0)^2+(\phi_m/\varepsilon_0)^2}\\ &= \alpha\lambda\frac{T}{\omega_E}\sum_m\left[1+\left(\frac{\omega_m-\omega_n}{\omega_E}\right)^2\right]^{-1}\frac{\phi_m\left\{(Z_m\omega_m/\varepsilon_0)^2+(\phi_m/\varepsilon_0)^2\right\}^{1/N}}{(Z_m\omega_m/\omega_E)^2+(\phi_m/\omega_E)^2},\end{aligned} \tag{6.22}$$

where $\lambda \equiv g^2p_{FB}^2/\pi\omega_E^2$ and $\alpha \equiv \pi/(N\sin(\pi/N))$. The equation for Z_n is

$$Z_n = 1+\alpha\lambda\frac{T}{\omega_E}\sum_m\left[1+\left(\frac{\omega_m-\omega_n}{\omega_E}\right)^2\right]^{-1}\frac{Z_m\omega_m\left\{(Z_m\omega_m/\varepsilon_0)^2+(\phi_m/\varepsilon_0)^2\right\}^{1/N}}{\omega_n(Z_m\omega_m/\omega_E)^2+(\phi_m/\omega_E)^2}. \tag{6.23}$$

There are now two energy scales, which the temperature is being compared to: phonon energy ω_E and the flat band energy ε_0. The flat band energy scale only appears inside the curly brackets under the Nth root and its importance is marginal when N is large. For $N \to \infty$, equations (6.4) and (6.5) are obtained as $\alpha \to 1$ and $\{x\}^{1/N} \to 1$.

What is the effect on superconductivity for finite N of these two different energy scales? We notice that ε can be taken out of the Nth root and included in the coupling. The equation for ϕ_n becomes

$$\phi_n = \tilde{\lambda}\frac{T}{\omega_E}\sum_m\left[1+\left(\frac{\omega_m-\omega_n}{\omega_E}\right)^2\right]^{-1}\frac{\phi_m}{\left\{(Z_m\omega_m/\omega_E)^2+(\phi_m/\omega_E)^2\right\}^{1-1/N}}, \tag{6.24}$$

with the coupling $\tilde{\lambda} = \alpha\lambda\left(\omega_E/\varepsilon_0\right)^{2/N}$. The equation for Z_n can also be transformed into

a similar form. Critical temperature can now be written in terms of $\tilde{\lambda}$ and ω_E as

$$T_c = f_N(\tilde{\lambda})\omega_E, \tag{6.25}$$

where f_N is some function whose shape depends on N.

The dependence of T_C on $\tilde{\lambda}$ for finite N is shown in Fig. 16 for different N. When $N = 2$ is the self-consistency equations have by coincidence the same form as in the usual metallic system, but with the interaction constant defined with different parameters. With $N > 2$ the number of layers seems to mostly affect the derivative of $T_C(\tilde{\lambda})$ at $\tilde{\lambda} \to 0$. For $N \to \infty$ the ideal flat band behaviour of Fig. 14a is regained.

6.5 Validity of the perturbation expansion

Migdal's theorem is used in Sec. 3.3 to approximate the full electron-phonon vertex Γ by its bare value g. The theorem says that in the perturbation theory, we can take $\lambda\omega_D/\varepsilon_F$ instead of just λ as the small expansion parameter, provided that $\omega_D \ll \varepsilon_F$. In a flat band $\varepsilon_F = 0$, so the assumptions of Migdal's theorem are not met. How do the conclusions change in the flat band, and when can the vertex corrections be neglected?

Using the Ward identity, Engelsberg and Schrieffer [37] have shown that Migdal's theorem actually also fails in metals in case of optical (Einstein) phonons with long wavelengths and that the correction to the vertex is of the order of λ as defined in Eq. (3.36), without the extra factor of ω_D/ε_F. In metals, the relative contribution of those phonons to the self-energy is small and in general Migdal's theorem stays valid[29]. In a flat band, the long-wavelength phonons are more important, and it is possible to modify the argument of Engelsberg and Schrieffer to get an estimate for the vertex corrections in this case.

The Ward identity is a self-consistency equation for the full vertex $\Gamma(p, q)$, where $p = (\omega, \mathbf{p})$ is the four-momentum of the incoming electron and $q = (\nu, \mathbf{q})$ is the four-momentum of the phonon. To illustrate the limits, we begin with a generalization of the Ward identity which is valid for $\mathbf{q} \to 0$, [37]

$$\frac{\nu\Gamma(\omega, \mathbf{p}; \nu, 0)}{g} = G^{-1}(\omega + \nu, \mathbf{p}) - G^{-1}(\omega, \mathbf{p}). \tag{6.26}$$

At $\nu \to 0$ we get

$$\begin{aligned} \frac{\Gamma(\omega, \mathbf{p}; 0, 0)}{g} &= \lim_{\nu\to 0} \frac{G^{-1}(\omega + \nu, \mathbf{p}) - G^{-1}(\omega, \mathbf{p})}{\nu} = \frac{\partial G^{-1}(\omega, \mathbf{p})}{\partial\omega} \\ &= \frac{\partial G_0^{-1}(\omega, \mathbf{p})}{\partial\omega} - \frac{\partial\Sigma(\omega)}{\partial\omega} = 1 - \frac{\partial\Sigma(\omega)}{\partial\omega}. \end{aligned} \tag{6.27}$$

To approximate the size of the vertex corrections with this, we first analytically evaluate the self-energy to the lowest order using the Einstein model for phonons. At zero

temperature it is

$$\begin{aligned}\Sigma(i\omega) &\approx \int \frac{\mathrm{d}^2\mathbf{p}}{(2\pi)^2}\int \frac{\mathrm{d}\omega'}{2\pi} g^2 D_E(i\omega - i\omega')G_0(i\omega') \\ &= \frac{g^2 p_{FB}}{4\pi}\, P\!\int_{-\infty}^{+\infty} \frac{\mathrm{d}\omega'}{2\pi} \frac{-2\omega_E}{\omega_E^2 + (\omega-\omega')^2}\frac{1}{i\omega}.\end{aligned} \tag{6.28}$$

Because at a finite temperature the Matsubara summation does not include zero frequencies, the integral over frequency is evaluated as a principal value integral. After the integration, the self-energy is found to be

$$\Sigma(i\omega) = \frac{\lambda}{2}\frac{\omega_E^2 i\omega}{\omega_E^2 + \omega^2}, \tag{6.29}$$

with $\lambda = g^2 p_{FB}/2\pi\omega_E^2$. This matches with the numerically obtained shape for $1 - Z(i\omega)$, which at low temperatures looks like a Lorentzian.

The self-energy can now be analytically continued to real frequencies on the upper half-plane by substitution $i\omega \to \omega + i\delta$, with $\delta \to 0+$. Taking the derivative, we have

$$\frac{\partial\Sigma(\omega)}{\partial\omega} = -\frac{\lambda}{2}\frac{\omega_E^2(\omega^2 + \omega_E^2)}{\left((\omega+i\delta)^2 - \omega_E^2\right)^2}, \tag{6.30}$$

which means that at low energies $\omega \ll \omega_E$, we find at $\mathbf{q} \to 0$ and $\nu \to 0$ from the Ward identity a vertex correction

$$\frac{\Gamma(\omega, \mathbf{p}; 0, 0)}{g} = 1 + \frac{\lambda}{2}, \tag{6.31}$$

where we did not take into account the fact that the vertex correction should be self-consistently included on the self-energy, so it would also appear on the rhs of the above equation. Thus, in order to accurately approximate the full vertex with the bare vertex, we must have $\lambda \ll 1$, and it would seem that there is no equivalent of the Migdal's theorem in a flat band.

For Debye phonons the calculation can be done in a similar fashion as in (6.15) and again the significant difference is the change of the phonon energy scale from ω_E to $\omega_0 = \omega_D p_{FB}/q_M$. At $\omega \to 0$ exactly the same result as with the Einstein phonons is obtained, but with λ as defined in Eq. (6.16).

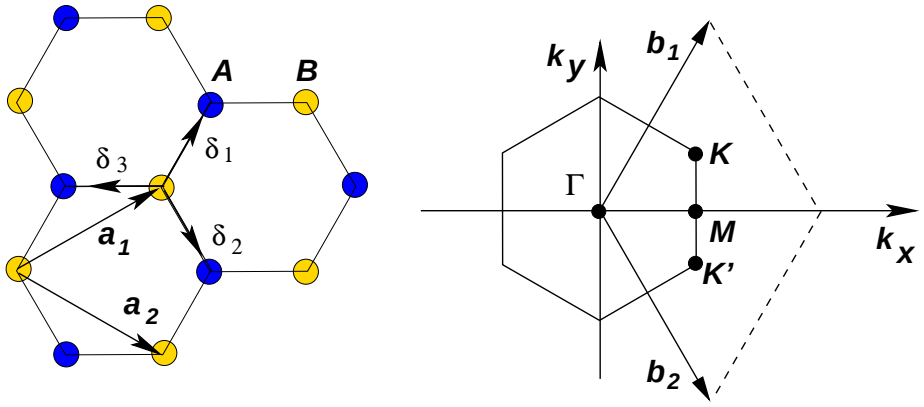

Figure 17. Left: Graphene lattice. Carbon atoms belonging to sublattices A and B have been colored blue and yellow, respectively. $\mathbf{a}_1, 2$ are the lattice vectors and $\boldsymbol{\delta}_{1,2,3}$ are the nearest neighbour vector relating the sublattices to each other. Right: 1st Brilloun zone of graphene. Dirac cones are at K and K'. $\mathbf{b}_{1,2}$ are the reciprocal lattice vectors. The figure is from [39].

7 Superconductivity on rhombohedral graphite

In this section, we show that the surface states of rhombohedral graphite realize the flat band dispersion described in the previous chapter. The presentation is based on the textbook by Heikkilä[38]. After this, I present the form the Eliashberg theory takes in the rhombohedral graphite and discuss how to solve it numerically. Before discussing rhombohedral graphite, I start from a single graphene layer and its Hamiltonian.

7.1 Electronic structure of a single graphene layer

In graphene carbon atoms are arranged in a two dimensional honeycomb lattice, which is a Bravais lattice with a two-point basis (Fig. 17). The basis defines two sublattices A and B, which can be described with two lattice vectors

$$\boldsymbol{a}_{1,2} = \frac{1}{2}(\mp\sqrt{3}, 3)a. \tag{7.1}$$

Above, a is the lattice spacing, for graphene $a = 1.42$. The nearest neighbours of an A-atom are three B-atoms and the nearest neighbours of a B-atom are three A-atoms. Nearest-neighbour vectors from an A-atom to a B-atom are

$$\boldsymbol{\delta}_1 = -\frac{1}{2}(\sqrt{3}, 1)a, \quad \boldsymbol{\delta}_2 = \frac{1}{2}(\sqrt{3}, -1)a, \quad \boldsymbol{\delta}_3 = (0, 1)a. \tag{7.2}$$

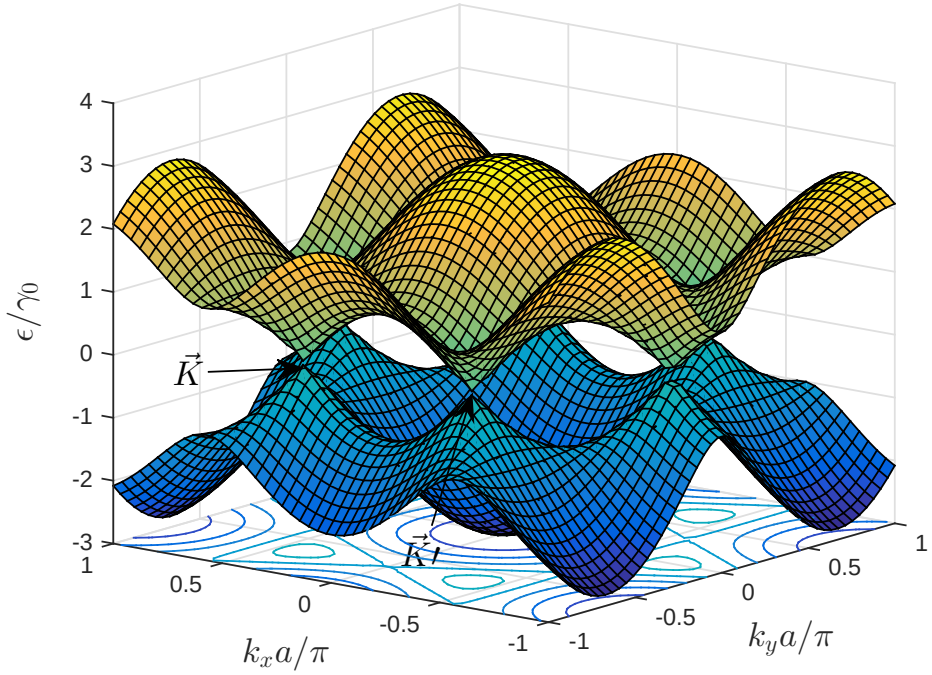

Figure 18. Dispersion of graphite. The Dirac cones are at points K and K'. the figure is taken from [40].

Using a tight-binding model, the coupling between the states localized at each lattice point can be described with a nearest-neighbour hopping energy γ_0. The tight-binding Hamiltonian for graphene, written in real space, is [38]

$$H_g = -\gamma_0 \sum_{\mathbf{R}} \psi(\mathbf{R})^\dagger \left[\psi(\mathbf{R}+\boldsymbol{\delta}_1) + \psi(\mathbf{R}+\boldsymbol{\delta}_2) + \psi(\mathbf{R}+\boldsymbol{\delta}_3)\right] + \text{h.c.}, \tag{7.3}$$

where $\psi(\mathbf{R})$ creates an electron in the state centered at position $\mathbf{R}$. The momentum-space representation is defined through Fourier transform:

$$c_{A,\mathbf{p}} = \frac{1}{\sqrt{N}} \sum_{\mathbf{R}} e^{i\mathbf{p}\cdot\mathbf{R}} \psi(\mathbf{R}), \quad c_{B,\mathbf{p}} = \frac{1}{\sqrt{N}} \sum_{\mathbf{R}} e^{i\mathbf{p}\cdot\mathbf{R}} \psi(\mathbf{R}+\boldsymbol{\delta}_3). \tag{7.4}$$

In momentum space the Hamiltonian is diagonal except for the mixing between the sublattices,

$$H_g = -\gamma_0 \sum_{\mathbf{p}} \gamma_{\mathbf{p}} c^\dagger_{A,\mathbf{p}} c_{B,\mathbf{p}} + \text{h.c.}, \tag{7.5}$$

where $\gamma_{\mathbf{p}} = 1 + e^{i\mathbf{p}\cdot\mathbf{a}_1} + e^{i\mathbf{p}\cdot\mathbf{a}_2}$. Collecting the operators from the two sublattices into 1×2 vectors, the Hamiltonian can be written as

$$H_g = -\gamma_0 \sum_{\mathbf{p}} \begin{pmatrix} 0 & \gamma_{\mathbf{p}} \\ \gamma^*_{\mathbf{p}} & 0 \end{pmatrix}. \tag{7.6}$$

Writing the eigenvalue equation for the above Hamiltonian, the dispersion of graphene

can be solved to be

$$\varepsilon(\mathbf{p}) = \pm\gamma_0|\gamma_{\mathbf{p}}| = \pm\gamma_0\left(3 + 2\cos\left(\sqrt{3}p_x a\right) + 4\cos\left(\frac{3p_y a}{2}\right)\cos\left(\frac{\sqrt{3}p_x a}{2}\right)\right)^{1/2}. \tag{7.7}$$

The dispersion is plotted in Fig. 18. The notable characteristic of graphene is the double-cone dispersion around certain points in momentum space, known as Dirac points. There are only two non-equivalent Dirac points, denoted with K and K'. These momenta are typically referred as valleys. The rest of the cones can be translated to those two with an addition of a reciprocal lattice vector.

A low-energy Hamiltonian is obtained from (7.6) by linearizing around the Dirac points:

$$H_g \approx v_F\begin{pmatrix} 0 & \pm p_x - ip_y \\ \pm p_x + ip_y & 0 \end{pmatrix}, \tag{7.8}$$

where $v_F = 3\gamma_0 a/2$ is the Fermi velocity near the Dirac point. Here, momentum is measured relative to point K/K'. The sign of p_x depends on the choice of the valley. Above, the coordinate system is chosen so that the positive sign corresponds to K and negative sign to K'. With Pauli matrices $\sigma_{x,y}$ acting on sublattice indices, the above expression can be further condensed to

$$H_g = v_F(\pm p_x\sigma_x + p_y\sigma_y). \tag{7.9}$$

This is the same form as the relativistic Hamiltonian for two-dimensional massless Dirac fermions, with $\pm$ standing for the choice of chirality, and the speed of light replaced with the Fermi velocity.

The cones in the graphene dispersion were already noticed in 1947 by P.R Wallace in a theoretical study of the electronic structure of graphene[41]. Wallace was mostly interested in studying graphene as part of graphite, and before 2004 it was generally believed that an isolated graphene layer would not be stable. However, in 2003 Andre Geim and Konstantin Novoselov succeeded in extracting single graphene layers from bulk graphite[42]. In 2005 they also managed to connect the graphene samples to electrodes and measure the Hall conductivity, which was found to be anomalous, suggesting that graphene has unique electrical properties[43]. Geim and Novoselov were awarded the 2010 Nobel prize in physics for their work on graphene.

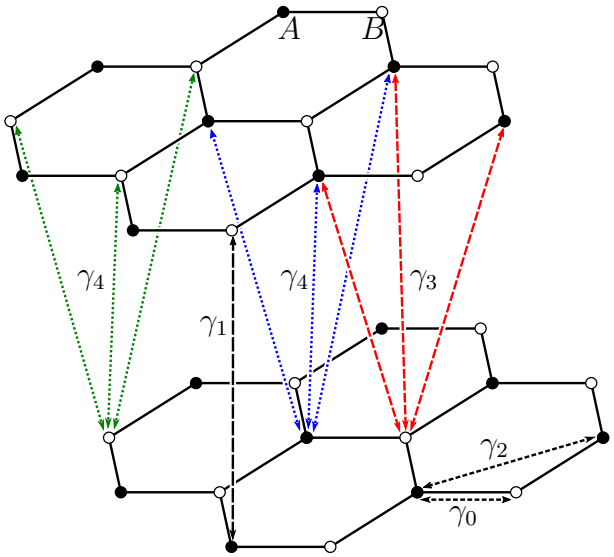

Figure 19. Parameters of the tight-binding model in rhombohedral graphite. γ_0 and γ_2 describe the hoppings inside a single graphene layer, whereas γ_1, γ_3 and γ_4 describe the hoppings between different layers. In this work, we only take into account γ_0 and γ_1, the effect of the other terms has been considered in [15] and the do not change the situation qualitatively, provided $\Delta \gg 2\gamma_1\gamma_4/\gamma_0$.

7.2 Electronic structure of rhombohedral graphite

Graphite is an allotrope of carbon composed from multiple graphene layers. There are two forms of ordered graphite, Bernal and rhombohedral graphite. Bernal is the most common form, but rhombohedral graphite also occurs in a metastable form. In these two forms the layers are arranged in different stackings, with different points of the subsequent layers being on top of each other.[38]

In the following, I concentrate on rhombohedral stacking with the stacking order ABC. This means that the upper layer is always shifted with a vector $\boldsymbol{\delta}_3$ with respect to the lower layer. The arrangement repeats itself every three layers because $3\boldsymbol{\delta}_3 = \mathbf{a}_1 + \mathbf{a}_2$ is a lattice vector. The reason we are interested in this specific arrangement of layers is because it has low-energy surface states with an approximate flat band. Henni et al. have experimentally verified that a rhombohedral graphite sample with 17 layers contains electronic bands with a flat dispersion[16].

Near the K point, the low energy Hamiltonian of rhombohedral graphite is[15]

$$H_{\mathrm{RHG}}(\mathbf{p}) = \begin{pmatrix} v_F(\mathbf{p}\cdot\boldsymbol{\sigma}) & \gamma_1\sigma_+ & & \\ \gamma_1\sigma_- & v_F(\mathbf{p}\cdot\boldsymbol{\sigma}) & \gamma_1\sigma_+ & \\ & \gamma_1\sigma_- & \ddots & \ddots \\ & & \ddots & \gamma_1\sigma_+ \\ & & \gamma_1\sigma_- & v_F(\mathbf{p}\cdot\boldsymbol{\sigma}) \end{pmatrix}, \tag{7.10}$$

which is a $N\times N$-matrix in terms of layer indices. In each layer, there is additionally the

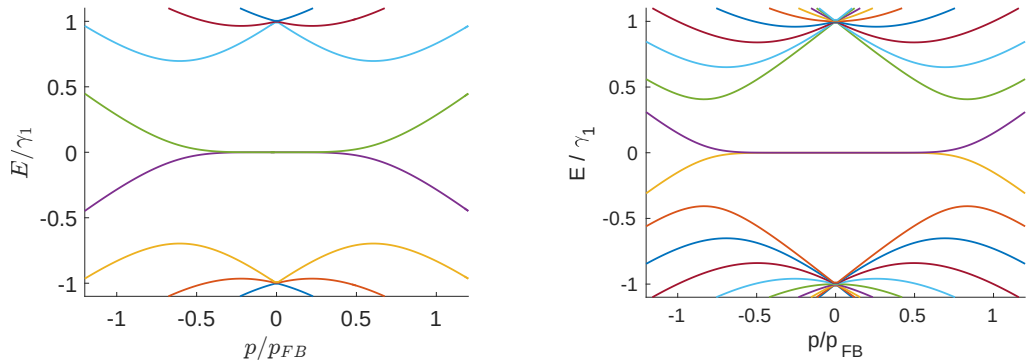

(a) $N = 5$ **(b)** $N = 10$

Figure 20. Low-energy dispersions for rhombohedral graphite with N layers with different N. The dispersion is very flat already for $N = 5$.

sublattice structure. Coupling between the layers is described by the ladder operators $\sigma_\pm$ and the strength of the coupling is γ_1. Inside the planes, carbon atoms are covalently bonded, but different layers are only held together with van der Waals bonds. Thus, $\gamma_1 \ll \gamma_0$. We take the values of the parameters to be $\gamma_0 = 3.2\,\text{eV}$ and $\gamma_1 = 0.39\,\text{eV}$[39], keeping in mind that these the values obtained for $\gamma_{0,1}$ in a seven-parameter model, and might not be accurate for our two-parameter model.

The Schrödinger equation for rhombohedral graphite is

$$(H_{\text{RHG}} - \varepsilon \mathbb{1})\,|\psi\rangle = 0, \tag{7.11}$$

where ε is the eigenenergy of the eigenvector $|\psi\rangle$. Components at each layer are denoted by 1×2 vectors $\check{\psi}_n$, where the check-sign is used to remind the reader of the sublattice structure. Numerically solved dispersion relations are shown in Fig. 20. The prominent feature of the dispersion is the low-energy states with weak dispersion. These correspond to surface states.

To study the Hamiltonian (7.10) analytically, we can write the solution as an recursion relation between the different layers:

$$\gamma_1\sigma_+\check{\psi}_{n-1} + [v_F(\mathbf{p}\cdot\boldsymbol{\sigma}) - \varepsilon\mathbb{1}]\,\check{\psi}_n + \gamma_1\sigma_-\check{\psi}_{n+1} = 0, \quad \text{for} \quad n \neq 1, N \tag{7.12}$$

As described in [44], the solutions for this kind of recurrence relation can be expressed in the form

$$\check{\psi}_n = A_1 r_1^n \check{\alpha}_1 + A_2 r_2^n \check{\alpha}_2, \tag{7.13}$$

where A_j are constants to be determined from the boundary conditions. In this case, the equations for the surfaces determine them. r_j and $\check{\alpha}_j$ are the eigenvalues and eigenvectors of the characteristic equation

$$\left(\gamma_1\check{\sigma}_+ + r\,[v_F(\mathbf{p}\cdot\check{\boldsymbol{\sigma}}) - \varepsilon\mathbb{1}] + r^2\gamma_1\check{\sigma}_-\right)\check{\alpha} = 0, \tag{7.14}$$

Inspecting the general form of the solution (7.13), it can be seen that if $|r| = 1$, the amplitude of the solution is the same on all layers. In that case, the state is delocalized over the whole crystal, and the solution describes a bulk solution. We can then choose $r_1 = e^{idq}$ and $r_2 = e^{-idq}$, with d being the distance between the layers and q the out-of-plane momentum. The solution has the familiar plane wave form.

On the other hand, if $|r| < 1$, the state decays when proceeding from the surface to the bulk. If we insist on writing the solution in terms of out-of-plane momentum q, we will have to generalize it to complex values: $q = q' + iq''$, where q' and q'' are real and $q'' > 0$. Now the amplitude of the solution on each layer is determined by

$$|r^n| = e^{-q''dn}, \tag{7.15}$$

which means that the state decays exponentially into the bulk. Had we chosen $|r| > 1$ ($q'' < 0$), the solution would be localized on the opposite surface.

Returning to the specific case of rhombohedral graphite, by defining $\tilde{p} = p/p_{FB}$, $p_{FB} = \gamma_1/v_F$, $\phi = -\arg(p_x + ip_y)$ and $\tilde{\varepsilon} = \varepsilon/\gamma_1$, Eq. (7.14) can be written as

$$\begin{bmatrix} -r\tilde{\varepsilon} & 1 - r\tilde{p}e^{-i\phi} \\ r^2 - r\tilde{p}e^{i\phi} & -r\tilde{\varepsilon} \end{bmatrix} \check{\alpha} = 0, \tag{7.16}$$

We can restrict the study to surface states by approximating $\varepsilon \approx 0$ in (7.16). Taking the determinant of the matrix in (7.16), the roots are then seen to be $r_1 \approx \tilde{p}e^{i\phi}$ and $r_2 \approx e^{i\phi}/\tilde{p}$. The solution is localized to the surfaces if $p \ll p_{FB}$. When $p \approx p_{FB}$, the state is spread over the whole crystal.

The vectors α corresponding to r_1 and r_2 are

$$\check{\alpha}_1 = \begin{bmatrix} 1 \\ \zeta e^{i\phi} \end{bmatrix}, \quad \check{\alpha}_2 = \begin{bmatrix} \zeta \\ e^{i\phi} \end{bmatrix}, \quad \text{with} \quad \zeta = \frac{\tilde{p}\,\tilde{\varepsilon}}{1 - |\tilde{p}|^2}, \tag{7.17}$$

so that the solution in each layer is

$$\check{\psi}_n = A_1 \tilde{p}^{\,n-1} \begin{bmatrix} 1 \\ \zeta e^{i\phi} \end{bmatrix} + A_2 \tilde{p}^{\,N-n} \begin{bmatrix} \zeta \\ e^{i\phi} \end{bmatrix}. \tag{7.18}$$

The equations for the surfaces couple A_1 and A_2:

$$[v_F(\mathbf{p} \cdot \boldsymbol{\sigma}) - \varepsilon \mathbb{1}]\, \check{\psi}_1 + \gamma_1 \sigma_- \check{\psi}_2 = 0, \tag{7.19}$$

$$[v_F(\mathbf{p} \cdot \boldsymbol{\sigma}) - \varepsilon \mathbb{1}]\, \check{\psi}_N + \gamma_1 \sigma_+ \check{\psi}_{N-1} = 0, \tag{7.20}$$

Substituting the solution (7.18) into these, we can solve the constants A_i and the energy ε. The first component of Eq. (7.19) and the second component of (7.20) equation reduce, respectively, to

$$A_1 \frac{\tilde{\varepsilon}}{1 - \tilde{p}^2} = A_2 \tilde{p}^N \quad \text{and} \quad A_2 \frac{\tilde{\varepsilon}}{1 - \tilde{p}^2} = A_1 \tilde{p}^N. \tag{7.21}$$

Solving $\tilde{\varepsilon}$ from this pair of equations, the dispersion relation is found be

$$\varepsilon_{\mathbf{p}} = \pm\xi_{\mathbf{p}} \left(1 - \frac{p^2}{p_{FB}^2}\right), \quad \text{with} \quad \xi_{\mathbf{p}} = \gamma_1 \left(\frac{p}{p_{FB}}\right)^N . \tag{7.22}$$

The surface states of rhombohedral graphite thus realize the flat band dispersion discussed in the previous chapter. The superficial difference to an ideal flat band system is the factor of $(1 - p^2/p_{FB}^2)$, which flattens the flat band even more at its boundaries. The more important difference is the fact the surface states are not localized to the surface and that the electron–phonon interaction couples them to other energy eigenstates. We must also keep in mind that the above is obtained near K valley and that there is there is a similar dispersion at K' valley. The two electrons bound to a Cooper pair occupy different valleys.

7.3 Surface superconductivity in the BCS model

The above derivation for the surface state spectrum can be extended for superconducting state within the BCS theory by replacing the Schrödinger equation with the Bogoliubov–de Gennes equations. This has been done by Heikkilä and Kopnin[15], and is not be presented here in detail. Some points of the derivation are presented, as they are important also for the Eliashberg derivation, and give some intuition about the possible superconductivity in rhombohedral graphite.

To write the Bogoliubov–de Gennes equations, we need the Hamiltonian for the time-reversed states (holes). The corresponding hole for the particle at valley K is situated in the valley K'. In spite of this, the hole Hamiltonian can be shown to coincide with the particle Hamiltonian, [15]

$$H_h(\mathbf{K}, \mathbf{p}) = H^*(-\mathbf{K}, -\mathbf{p}) = H(\mathbf{K}, \mathbf{p}). \tag{7.23}$$

The Bogoliubov–de Gennes equations are

$$\sum_m \tau_3 \otimes H_{nm}(\mathbf{K}, \mathbf{p}) \breve{\Psi}_m + \breve{\Delta}_n \breve{\Psi}_n = \varepsilon \breve{\Psi}_n. \tag{7.24}$$

The above equation has a similar structure as the Schrödinger equation for the normal state, and the same method as used for Eq. (7.11) can be used to solve it, the only difference being the extra Nambu dimension in the matrices and vectors.

What is the form of the order parameter in the sublattice space? In both valleys, the surface states of sublattices A and B are localized at surfaces $n = 1$ and $n = N$, respectively. As the graphene layers are weakly coupled as compared to the coupling inside the layer, the phonon-mediated interaction mainly happens between the electronic states localized in the same plane. The attractive interaction leading to surface superconductivity thus happens between the surface states at the opposite valleys. Because in the sublattice A the surface states are localized at the surface n=1 in both valleys (for sublattice B, at

the surface n=N), the order parameter Δ is diagonal in sublattice space.

Assuming that Δ is non-zero only at the surfaces, and $N \to \infty$ so that the two surfaces decouple, a self-consistency equation for Δ can be obtained, [15]

$$\Delta = \frac{W}{d} \int_{p<p_{FB}} \frac{\mathrm{d}^2 p}{(2\pi)^2} \frac{(1 - p^2/p_{FB}^2)^2 \Delta}{\sqrt{|\Delta|^2 (1 - p^2/p_{FB}^2)^2}} \times \tanh \frac{|\Delta|(1 - p^2/p_{FB}^2)}{2T}, \tag{7.25}$$

where W is the 3D coupling potential and d is the distance between the layers. This equation differs from the self-consistency equation for metals by the presence of the normalization factors $(1 - p^2/p_{FB}^2)$ connected to the delocalization of the surface states. At zero temperature, Eq. (7.25) reduces to

$$\Delta_0 = \frac{g}{8\pi}, \tag{7.26}$$

with the coupling energy $g = W p_{FB}^2/d$. As in the case of the flat band, the above Δ_0 is linear in g. The critical temperature is determined from Eq. (7.25) by taking $\Delta \to 0$. The result is $\Delta_0 = 3k_B T_C$ [15]. Here it should be noted that in this result the normalization factor plays a role: for an ideal flat band we would have $\Delta_0 = 2k_B T_C$. Neglecting the details of the rhombohedral graphite and idealizing it as a simple flat band dispersion thus gives qualitatively similar, but not exactly correct results.

7.4 Eliashberg theory for rhombohedral graphite

To my knowledge, Eliashberg theory has not been done before for rhombohedral graphite, so the derivations in this section are new. To write the Eliashberg equations for rhombohedral graphite, we first consider the normal state and then generalize to the superconducting state. The phonon-mediated interaction couples the valleys, so we need to consider both of them. To express the Hamiltonian in valley K' in terms of the Hamiltonian in the valley K, we use the symmetry [39]

$$H_{\mathrm{RHG}}(-\mathbf{K}, \bar{\mathbf{p}}) = H_{\mathrm{RHG}}(\mathbf{K}, \mathbf{p}), \tag{7.27}$$

where $\bar{\mathbf{p}} = (-p_x, p_y)$ and σ_z act on the sublattice space. We need the "non-interacting" propagators in the valleys,

$$G_0^{-1}(\mathbf{K}, \mathbf{p}, i\omega_n) = i\omega_n \mathbb{1} - H_{\mathrm{RHG}}(\mathbf{K}, \mathbf{p}), \tag{7.28}$$

$$G_0^{-1}(-\mathbf{K}, \bar{\mathbf{p}}, i\omega_n) = i\omega_n \mathbb{1} - H_{\mathrm{RHG}}(-\mathbf{K}, \bar{\mathbf{p}}). \tag{7.29}$$

The above propagators are non-interacting in the sense that even though they contain the hopping interactions, electron–phonon interaction is not included. Using Eq. (7.27) we have

$$G_0^{-1}(-\mathbf{K}, \bar{\mathbf{p}}, i\omega_n) = G_0^{-1}(\mathbf{K}, \mathbf{p}, i\omega_n). \tag{7.30}$$

The above propagators are $2N\times 2N$ matrices with N the number of graphene layers and 2 coming from the sublattice structure. They are diagonal in the in-plane momentum and have a non-diagonal layer and sublattice structure. This structure can be written explicitly as

$$G_0^{-1}(\mathbf{K},\mathbf{p},i\omega_n)_{ij} = i\omega_n \mathbb{1}\delta_{ij} - v_F(\mathbf{p}\cdot\boldsymbol{\sigma})\delta_{ij} - \gamma_1\sigma_+\delta_{i,j+1} - \gamma_1\sigma_-\delta_{i,j-1}. \tag{7.31}$$

Interacting propagators are obtained by adding the self-energy from the electron–phonon interaction,

$$G^{-1}(\mathbf{K},\mathbf{p},i\omega_n) = G_0^{-1}(\mathbf{K},\mathbf{p},i\omega_n) - \Sigma(\mathbf{K},\mathbf{p},i\omega_n), \tag{7.32}$$
$$G^{-1}(-\mathbf{K},\bar{\mathbf{p}},i\omega_n) = G_0^{-1}(-\mathbf{K},\bar{\mathbf{p}},i\omega_n) - \Sigma(-\mathbf{K},\bar{\mathbf{p}},i\omega_n). \tag{7.33}$$

Graphene layers are weakly coupled together, so as an approximation we can limit the phonons to only propagate within the layers, and not across them. With this kind of interaction, the Hamiltonian and the self-energy cannot be diagonalized at the same time, because the electronic states are not localized within a certain layer. Electron–phonon interaction tends to mix the electronic eigenstates. This mixing becomes weak for $N\to\infty$ and $p < p_{FB}$.

The in-plane propagation of phonons is enforced by adding a δ_{ij}-term in the phonon propagator. In Dyson's equation [Eq. (3.33)] the 3D integration over momentum is replaced by an integration over in-plane 2D momentum and a sum over the planes. We get

$$\begin{aligned}\Sigma(\mathbf{p},i\omega_n)_{ij} &= T\sum_m \sum_{k=1}^{N} \int_{\mathrm{BZ}} \frac{\mathrm{d}^2\mathbf{p}'}{(2\pi)^2} g^2 D(\mathbf{p}-\mathbf{p}', i\omega_n - i\omega_m)\delta_{ik} G(\mathbf{p}', i\omega_m)_{kj} \\ &= T\sum_m \int_{\mathrm{BZ}} \frac{\mathrm{d}^2\mathbf{p}'}{(2\pi)^2} g^2 D(\mathbf{p}-\mathbf{p}', i\omega_n - i\omega_m) G(\mathbf{p}', i\omega_m)_{ij},\end{aligned} \tag{7.34}$$

where i and j are the layer indices. In this equation, the integral is over the whole Brilloun zone, and correspondingly, the self-energy and the propagator are not the ones defined only in the valleys.

To use the low-energy expansion, we break up the integration into two parts corresponding to the two valleys. This is possible because $G(\mathbf{p},i\omega_n)\neq 0$ only when $\mathbf{p}\sim\mathbf{K},\mathbf{K}'$. For valley K, we get

$$\begin{aligned}\Sigma(\mathbf{K},\mathbf{p},i\omega_n) = T\sum_m \int_{p<p_c} \frac{\mathrm{d}^2\mathbf{p}'}{(2\pi)^2} \Big[& g^2 D(\mathbf{p}-\mathbf{p}', i\omega_n - i\omega_m) G(\mathbf{K},\mathbf{p}', i\omega_m) \\ & + g^2 D(\mathbf{K}-\mathbf{K}'+\mathbf{p}-\mathbf{p}', i\omega_n - i\omega_m) G(-\mathbf{K},\mathbf{p}', i\omega_m)\Big],\end{aligned} \tag{7.35}$$

where the momentum $\mathbf{p}$ is now measured relative to the $\mathbf{K}$. The above expression is valid for $\mathbf{p}\ll|\mathbf{K}-\mathbf{K}'|$. A cutoff p_c needs to be specified in this case. The self-energy in valley

K' is

$$\Sigma(-\mathbf{K},\bar{\mathbf{p}},i\omega_n)_{=}T\sum_m\int_{p<p_c}\frac{\mathrm{d}^2\mathbf{p}'}{(2\pi)^2}\Big[g^2D(\mathbf{K}'-\mathbf{K}+\bar{\mathbf{p}}-\mathbf{p}',i\omega_n-i\omega_m)G(\mathbf{K},\mathbf{p}',i\omega_m) + g^2D(\mathbf{p}-\mathbf{p}',i\omega_n-i\omega_m)G(-\mathbf{K},\bar{\mathbf{p}}',i\omega_m)\Big], \tag{7.36}$$

where the facts that $|\bar{\mathbf{p}}-\bar{\mathbf{p}}'|=|\mathbf{p}-\mathbf{p}'|$ and that the phonon propagator only depends on the magnitude of the momentum were used. Because

$$|\mathbf{K}-\mathbf{K}'+\mathbf{p}-\bar{\mathbf{p}}'|=|\mathbf{K}'-\mathbf{K}+\bar{\mathbf{p}}-\mathbf{p}'|, \tag{7.37}$$

we can write Eq. (7.35) as

$$\Sigma(\mathbf{K},\mathbf{p},i\omega_n)=T\sum_m\int_{p<p_c}\frac{\mathrm{d}^2\mathbf{p}'}{(2\pi)^2}\Big[g^2D(\mathbf{p}-\mathbf{p}',i\omega_n-i\omega_m)G(\mathbf{K},\mathbf{p}',i\omega_m) +g^2D(\mathbf{K}'-\mathbf{K}+\bar{\mathbf{p}}-\mathbf{p}',i\omega_n-i\omega_m)G(-\mathbf{K},\bar{\mathbf{p}}',i\omega_m)\Big]. \tag{7.38}$$

We now assume the symmetry of the solution as the symmetry of the Hamiltonian, $\Sigma(-\mathbf{K},\bar{\mathbf{p}})=\Sigma(\mathbf{K},\mathbf{p})$, and $G(-\mathbf{K},\bar{\mathbf{p}})=G(\mathbf{K},\mathbf{p})$. This choice corresponds to s-wave superconductivity. We see that in this case Eqs. (7.38) and (7.36) are equivalent and reduce to

$$\Sigma(\mathbf{K},\mathbf{p},i\omega_n)=T\sum_m\int_{p<p_c}\frac{\mathrm{d}^2\mathbf{p}'}{(2\pi)^2}\Big[g^2D(\mathbf{p}-\mathbf{p}',i\omega_n-i\omega_m) + g^2D(\mathbf{K}'-\mathbf{K}+\bar{\mathbf{p}}-\mathbf{p}',i\omega_n-i\omega_m)\Big]G(\mathbf{K},\mathbf{p},i\omega_m). \tag{7.39}$$

In the Einstein phonon model, the propagator has no momentum dependence, and we can add the phonon propagators together,

$$\Sigma(\mathbf{K},i\omega_n)=T\sum_m 2g^2D_E(i\omega_n-i\omega_m)\int_{p<p_c}\frac{\mathrm{d}^2\mathbf{p}'}{(2\pi)^2}G(\mathbf{K},\mathbf{p},i\omega_m). \tag{7.40}$$

With the Einstein model, the existence of the valleys shows up only as a factor of 2. Thus, the valley structure of rhombohedral graphite flat bands does not change the form of the equations as compared to the one flat-band case we study in Sec. 6.

In the Debye phonon model, we can remove the momentum dependence from the intervalley propagator. The distance between K and K', reduced to the first Brilloun zone, is $|\mathbf{K}-\mathbf{K}'|=4\pi/3\sqrt{3}a$. Because the size of the flat band is much smaller than the distance between the valleys,

$$\frac{p_{FB}}{|\mathbf{K}-\mathbf{K}'|}=\frac{\gamma_0}{\gamma_1}\frac{\sqrt{3}}{2\pi}\approx 0.03, \tag{7.41}$$

the interaction strength does not depend much on the exact momenta $\mathbf{p}$ and $\mathbf{p}'$ within the

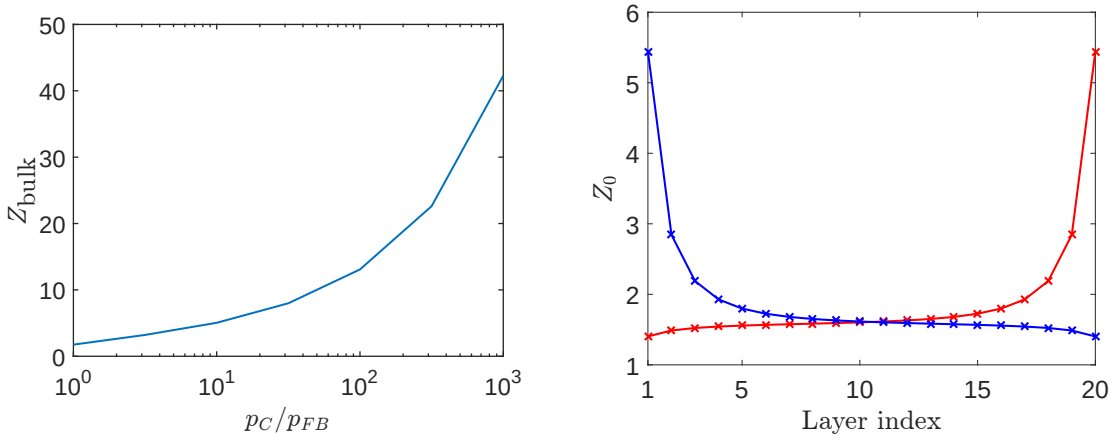

(a) **(b)**

Figure 21. Left: Dependence of the bulk Z on the momentum cutoff p_c with $\lambda = 0.5$ and 5 layers. The scale is logarithmic. Right: $Z(i\omega_0)$ on different layers with $\lambda = 0.5$, $p_c = p_{FB}$ and 20 graphene layers. The blue and the red curves are the magnitude of Z in the sublattices A and B, respectively.

flat band. We can then approximate the phonon momentum with the distance between the valleys,

$$g^2 D(\mathbf{K}-\mathbf{K}'+\mathbf{p}+\mathbf{p}', i\omega_n - i\omega_m) \approx g^2 D(\mathbf{K}-\mathbf{K}', i\omega_n - i\omega_m). \tag{7.42}$$

In the intravalley term, the momentum dependence is more important. Based on the approximations of Sec. 6.2, the effective coupling inside the valley is stronger than the coupling between the valleys, but the range of the interaction in frequency space is also smaller.

Assuming a momentum-independent interaction kernel, either from the Einstein model, or as some approximation of the Debye spectrum, we replace $g^2 D$'s with λ. Then the momentum dependence of the self-energy disappears. To see how the layers mix up with each other in the above equation, we write G in terms of the self-energy,

$$\Sigma(i\omega_n) = T \sum_m \lambda(i\omega_n - i\omega_m) \int_{p<p_c} \frac{\mathrm{d}^2\mathbf{p}}{(2\pi)^2} \left[G_0^{-1}(\mathbf{K}, \mathbf{p}, i\omega_m) - \Sigma(i\omega_m) \right]^{-1}. \tag{7.43}$$

When $p/p_{FB} \ll 1$, the surface states are well localized and the inverted matrix is almost diagonal. When $p/p_{FB} \sim 1$, the surface states delocalize across the layers and the inverted matrix is dense.

The above equation can now be solved numerically with the fixed-point iteration. In the normal state, we can begin with the ansatz $\Sigma = 0$. Then, to calculate the lhs of Eq. (7.43), the 2D momentum integral has to be first calculated for different ω_m. Every function evaluation in the integral involves calculating a matrix inverse of a $2N \times 2N$ matrix, so with increasing N, or with decreasing temperatures and many Matsubara frequencies, this soon becomes numerically expensive. After the integration, the sum over m with the interaction kernel λ is calculated.

Results from the numerics for the normal state are shown in Fig. 21. Below, with a bulk value, we mean the value of Z in the middle layer. We have not projected out the high-energy bulk states from the Hamiltonian, and propably for this reason, the bulk self-energy seems to diverge logarithmically with the momentum cutoff p_c. The value obtained for Z at surfaces differs from the bulk value. The even component of the self-energy, χ, seems to vanish in the numerical results. This is consistent with the analytical results from the ideal flat band.

Again, the transition to superconductivity is achieved by doubling the size of the matrices with Nambu structure. The non-interacting propagator becomes

$$\mathbf{G}_0^{-1}(\mathbf{K}, \mathbf{p}, i\omega_n) = i\omega_n \mathbb{1} - \tau_3 H_{\mathrm{RHG}}(\mathbf{K}, \mathbf{p}), \tag{7.44}$$

where the same Hamiltonian can be used for the particles and holes because of the relation (7.23). The interacting Hamiltonian is

$$\begin{aligned} \mathbf{G}^{-1}(\mathbf{K}, \mathbf{p}, i\omega_n) &= \mathbf{G}_0^{-1}(\mathbf{K}, \mathbf{p}, i\omega_n) - \mathbf{\Sigma}(i\omega_n) \\ &= Z(i\omega_n) i\omega_n \mathbb{1} - \tau_1 \phi(i\omega_n) - \tau_3 H_{\mathrm{RHG}}(\mathbf{K}, \mathbf{p}), \end{aligned} \tag{7.45}$$

where the χ-component is assumed to vanish. In the numerics, there is no need to do this assumption. Again, Z and ϕ are $2N \times 2N$ matrices, so $\mathbf{G}(\mathbf{p}, i\omega_n)$ is now $4N \times 4N$. Finally, the self-energy is calculated as

$$\mathbf{\Sigma}(i\omega_n) = T \sum_m \lambda(i\omega_m - i\omega_n) \int_{p<p_c} \frac{\mathrm{d}^2\mathbf{p}}{(2\pi)^2} \tau_3 \left[\mathbf{G}_0^{-1}(\mathbf{K}, \mathbf{p}, i\omega_m) - \mathbf{\Sigma}(i\omega_m) \right]^{-1} \tau_3, \tag{7.46}$$

with the only difference to Eq. (7.43) being the presence of the τ_3's, the effect of which is to flip the signs of the off-diagonal Nambu elements.

Eq. (7.46) is the Eliashberg equation for rhombohedral graphite and it can be solved numerically with minor modifications to the procedure described above for the normal state. A non-zero initial value for ϕ has to be assumed.

We can find an approximate solution to Eq. (7.46) by projecting out the high-energy bulk states (see Fig. 20). We are then left with one flat band state on either surface. Assuming that the number of layers is large, so that the surface states are not coupled, we get two decoupled equations for the two surfaces. In this case the sublattice structure is not important any more, and we can use the results for the ideal flat bands from the Sec. 6. The weak point of this argument is the delocalization of the surface states, which makes also the BCS results for rhombohedral graphite to differ from the results obtained in the ideal flat band.

In Fig. 21 the magnitude of the normal state self-energy seems to very large as compared to the values obtained for Z in the Fermi surface or the ideal flat band. The high cost of the numerics in terms of CPU time also forces us to solve the equations in relatively high temperatures. Within the temperatures available to us, I could not find a combination of parameters which would support superconductivity. In the other mod-

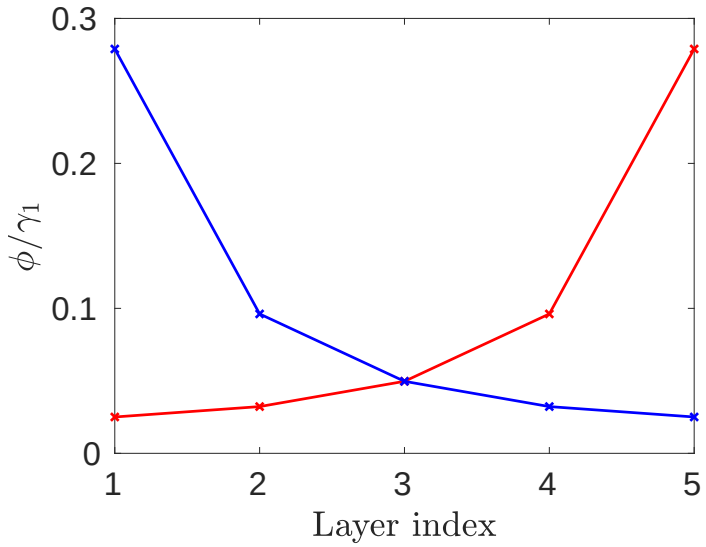

Figure 22. Magnitude of ϕ at different layers, with Z set to 1 and the parameters $\lambda = 0.2$, $\omega_E = 0.1\gamma_1$, $T = 0.01\omega_E$ and $p_c = p_{FB}$. The number of graphene layers was 5. ϕ is supported by the surface states and varies the same way as Z from layer to layer.

els considered in this thesis, superconductivity could be found at high temperatures by increasing the coupling. However, in rhombohedral graphite, Z seems to grow very fast with increasing λ and this may suppress superconductivity in the model.

To test the assumption that Z suppresses ϕ, I solved the Eliashberg equation (7.46) by setting $Z = 1$ at each iteration. In this case superconductivity appeared within accessible temperatures with any combination of parameters tested. The magnitude of ϕ varies from layer to layer the same way as Z (Fig. 22). Therefore, in this case Z seems to be more important than usual and in future work, it should be checked whether the Z obtained from the low-energy Hamiltonian agrees with the one found from a more complete Hamiltonian. The calculation of the transition temperature in rhombohedral graphite is also left for future work.

8 Conclusion

In this work, I study electron-phonon superconductivity in the Eliashberg theory. I review the Eliashberg theory for the Fermi surface and apply it to the flat band. I show that the flat band supports a parametrically enhanced superconductivity also in the Eliashberg theory and not only in the BCS theory. Because of this enhancement, materials with flat bands are promising candidates for high-temperature (even room-temperature) superconductivity. It is this prospect which makes their study worthwhile. The possible material with high-temperature surface superconductivity could be used to build new kinds of electrical components with much improved energy efficiency.

We study surface states of rhombohedral graphite as an example of a flat band system. This is motivated by the high temperature superconducting regions observed in a highly-ordered graphite samples with internal interfaces[14]. We write the Eliashberg equation for the rhombohedral graphite. The study is not finished as the superconducting gap and the transition temperature are still to be calculated. The role of the normal state self-energy from the phonon-mediated interaction in rhombohedral graphite also needs to be clarified.

Rhombohedral graphite is not the only possible system in which flat bands are obtained, as they have been predicted also in strained Dirac materials, heavy fermion compounds, transition metal oxides and anti-perovskites[45]. BCS superconductivity has been predicted to occur at least in a strained graphene[46]. The Eliashberg theory could be used to elucidate this prediction also.

In this thesis we have not considered the possibility of a magnetic order, but have concentrated only on superconductivity. A magnetic order is at odds with the superconducting s-wave order, so this possibility should be examined in detail. For example, rhombohedral graphite has recently been proposed to exhibit magnetic order[47]. Which one of these competing orderings is realized depends on the parameters describing the electron-phonon interaction and the Coulomb interaction. Therefore, the parameter space of the flat-band model should be charted to produce a complete phase diagram. This aspect is important as we search for the most promising candidates for high-temperature superconductivity.

References

[1] E. Maxwell. "Isotope effect in the superconductivity of mercury". *Physical Review* **78** (1950), p. 477.

[2] C. Reynolds et al. "Superconductivity of isotopes of mercury". *Physical Review* **78** (1950), p. 487.

[3] H. Fröhlich. "Isotope effect in superconductivity". *Proceedings of the Physical Society. Section A* **63** (1950), p. 778.

[4] H. Fröhlich. "Theory of the superconducting state. I. The ground state at the absolute zero of temperature". *Physical Review* **79** (1950), p. 845.

[5] J. Bardeen and D. Pines. "Electron-phonon interaction in metals". *Physical Review* **99** (1955), p. 1140.

[6] J. Bardeen, L. N. Cooper, and J. R. Schrieffer. "Theory of superconductivity". *Physical Review* **108** (1957), p. 1175.

[7] A. Migdal. "Interaction between electrons and lattice vibrations in a normal metal". *Soviet Physics, JETP* **7** (1958), pp. 996–1001.

[8] G. Éliashberg. "Interactions between electrons and lattice vibrations in a superconductor". *Soviet Physics, JETP* **11** (1960), pp. 696–702.

[9] Y. Nambu. "Quasi-particles and gauge invariance in the theory of superconductivity". *Physical Review* **117** (1960), p. 648.

[10] N. N. Bogoliubov, V. V. Tolmachev, and D. V. Shirkov. *A new method in the theory of superconductivity*. Consultants Bureau, New York, London, Chapman and Hall, 1959.

[11] P. Morel and P. Anderson. "Calculation of the superconducting state parameters with retarded electron-phonon interaction". *Physical Review* **125** (1962), p. 1263.

[12] T. T. Heikkilä, N. B. Kopnin, and G. E. Volovik. "Flat bands in topological media". *JETP letters* **94** (2011), pp. 233–239.

[13] T. Scheike et al. "Can doping graphite trigger room temperature superconductivity? Evidence for granular high-temperature superconductivity in water-treated graphite powder". *Advanced Materials* **24** (2012), pp. 5826–5831.

[14] A. Ballestar et al. "Josephson-coupled superconducting regions embedded at the interfaces of highly oriented pyrolytic graphite". *New Journal of Physics* **15** (2013), p. 023024.

[15] N. B. Kopnin and T. T. Heikkilä. "Surface superconductivity in rhombohedral graphite". In: *Carbon-based Superconductors: Towards High-Tc Superconductivity*. Ed. by J. Haruyama. Pan Stanford, 2014, pp. 231–263.

[16] Y. Henni et al. "Rhombohedral multilayer graphene: A magneto-Raman scattering study". *Nano Letters* **16** (2016), pp. 3710–3716.

[17] R. van Leeuwen. "First-principles approach to the electron-phonon interaction". *Physical Review B* **69** (2004), p. 115110.

[18] N. W. Ashcroft and N. D. Mermin. *Solid state physics*. New York: Holt, Rinehart and Winston, 1976.

[19] R. Ojajärvi. "Elektroni–fononi-vuorovaikutuksesta, suprajohtavuudesta ja grafeenista". Undergraduate research training assingment. 2016.

[20] G. Stefanucci and R. Van Leeuwen. *Nonequilibrium many-body theory of quantum systems: a modern introduction*. Cambridge University Press, 2013.

[21] A. Fetter and J. Walecka. *Quantum theory of many-particle systems*. New York: McGraw-Hill, 1971.

[22] L. D. Landau, E. M. Lifshitz, and L. P. Pitaevskij. *Statistical Physics. Part 2, Theory of the Condensed State*. 2nd ed. Course of Theoretical Physics. Oxford: Pergamon Press, 1980.

[23] H. Vidberg and J. Serene. "Solving the Eliashberg equations by means of N-point Padé approximants". *Journal of Low Temperature Physics* **29** (1977), pp. 179–192.

[24] F. Marsiglio, M. Schossmann, and J. Carbotte. "Iterative analytic continuation of the electron self-energy to the real axis". *Physical Review B* **37** (1988), p. 4965.

[25] A. Abrikosov, L. P. Gor'kov, and I. Y. Dzyaloshnskii. *Quantum field theoretical methods in statistical physics*. 2nd ed. Oxford: Pergamon Press, 1965.

[26] F. Marsiglio and J. Carbotte. "Electron-phonon superconductivity". In: *Superconductivity*. Springer, 2008, pp. 73–162.

[27] L. Hedin and S. Lundqvist. "Effects of electron-electron and electron-phonon interactions on the one-electron states of solids". *Solid state physics* **23** (1970), pp. 1–181.

[28] D. Scalapino, J. Schrieffer, and J. Wilkins. "Strong-coupling superconductivity. I". *Physical Review* **148** (1966), p. 263.

[29] G. Grimvall. *The electron-phonon interaction in metals*. Series of monographs on selected topics in solid state physics. Amsterdam: North-Holland Publishing Company, 1981.

[30] H. Bruus and K. Flensberg. *Many-Body quantum theory in condensed matter physics: An introduction*. Oxford University Press, 2004.

[31] F. Marsiglio. "Eliashberg theory of the critical temperature and isotope effect. Dependence on bandwidth, band-filling, and direct Coulomb repulsion". *Journal of Low Temperature Physics* **87** (1992), pp. 659–682.

[32] J. Carbotte. "Properties of boson-exchange superconductors". *Reviews of Modern Physics* **62** (1990), p. 1027.

[33] M. S. Scheurer. "Mechanism, time-reversal symmetry, and topology of superconductivity in noncentrosymmetric systems". *Physical Review B* **93** (2016), p. 174509.

[34] J. R. Schrieffer. *Theory of superconductivity*. 3rd pr., rev. Reading, Massachusetts: Perseus Books, 1983.

[35] Y. V. Nazarov and J. Danon. *Advanced Quantum Mechanics*. Cambridge University Press, 2013.

[36] R. Drost et al. "Topological states in engineered atomic lattices". *Nature Physics* (2017).

[37] S. Engelsberg and J. R. Schrieffer. "Coupled Electron-Phonon System". *Physical Review* **131** (3 1963), pp. 993–1008.

[38] T. T. Heikkilä. *The Physics of Nanoelectronics*. Oxford University Press, 2013.

[39] A. C. Neto et al. "The electronic properties of graphene". *Reviews of Modern Physics* **81** (2009), p. 109.

[40] T. Moisala. "Topological properties of mono-and multilayer graphene, flat bands and surface superconductivity". Master's thesis. 2015.

[41] P. R. Wallace. "The band theory of graphite". *Physical Review* **71** (1947), p. 622.

[42] K. S. Novoselov et al. "Electric field effect in atomically thin carbon films". *Science* **306** (2004), pp. 666–669.

[43] K. S. Novoselov et al. "Two-dimensional gas of massless Dirac fermions in graphene". *Nature* **438** (2005), pp. 197–200.

[44] A.-B. Chen, Y.-M. Lai-Hsu, and W. Chen. "Difference-equation approach to the electronic structures of surfaces, interfaces, and superlattices". *Phys. Rev. B* **39** (2 1989), pp. 923–929.

[45] E. Tang and L. Fu. "Strain-induced partially flat band, helical snake states and interface superconductivity in topological crystalline insulators". *Nature Physics* **10** (2014), pp. 964–969.

[46] V. Kauppila, F. Aikebaier, and T. Heikkilä. "Flat-band superconductivity in strained Dirac materials". *Physical Review B* **93** (2016), p. 214505.

[47] B. Pamuk et al. "Magnetic gap opening in rhombohedral-stacked multilayer graphene from first principles". *Physical Review B* **95** (2017), p. 075422.